MINISTÉRIO DA CIÊNCIA, TECNOLOGIA E INOVAÇÕES
INSTITUTO NACIONAL DE PESQUISAS ESPACIAIS

sid.inpe.br/mtc-m21d/2022/11.01.17.43.35-TDI

COSMIC CHEMICAL EVOLUTION: MODELING AND COMPARING WITH OBSERVATIONS

Lia Camargo Corazza

Doctorate Thesis of the Graduate Course in Astrophysics, guided by Drs. Oswaldo Duarte Miranda, and Carlos Alexandre Wuensche de Souza, approved in October 04, 2022.

URL of the original document:
<http://urlib.net/8JMKD3MGP3W34T/47TD3RG>

INPE
São José dos Campos
2022

PUBLISHED BY:

Instituto Nacional de Pesquisas Espaciais - INPE
Coordenação de Ensino, Pesquisa e Extensão (COEPE)
Divisão de Biblioteca (DIBIB)
CEP 12.227-010
São José dos Campos - SP - Brasil
Tel.:(012) 3208-6923/7348
E-mail: pubtc@inpe.br

MINISTÉRIO DA CIÊNCIA, TECNOLOGIA E INOVAÇÕES
INSTITUTO NACIONAL DE PESQUISAS ESPACIAIS

sid.inpe.br/mtc-m21d/2022/11.01.17.43.35-TDI

COSMIC CHEMICAL EVOLUTION: MODELING AND COMPARING WITH OBSERVATIONS

Lia Camargo Corazza

Doctorate Thesis of the Graduate Course in Astrophysics, guided by Drs. Oswaldo Duarte Miranda, and Carlos Alexandre Wuensche de Souza, approved in October 04, 2022.

URL of the original document:
<http://urlib.net/8JMKD3MGP3W34T/47TD3RG>

INPE
São José dos Campos
2022

Cataloging in Publication Data

Corazza, Lia Camargo.

Co81c Cosmic chemical evolution: modeling and comparing with observations / Lia Camargo Corazza. – São José dos Campos : INPE, 2022.

xviii + 70 p. ; (sid.inpe.br/mtc-m21d/2022/11.01.17.43.35-TDI)

Thesis (Doctorate in Astrophysics) – Instituto Nacional de Pesquisas Espaciais, São José dos Campos, 2022.

Guiding : Drs. Oswaldo Duarte Miranda, and Carlos Alexandre Wuensche de Souza.

1. Chemical evolution. 2. Cosmic abundances. 3. First Stars. I.Title.

CDU 52-5

MINISTÉRIO DA CIÊNCIA, TECNOLOGIA E INOVAÇÕES

INSTITUTO NACIONAL DE PESQUISAS ESPACIAIS
Serviço de Pós-Graduação - SEPGR

DEFESA FINAL DE TESE DE LIA CAMARGO CORAZZA
BANCA Nº 268/2022, REG. 133949/2017

No dia 04 de outubro de 2022, às 10h, por teleconferência, o(a) aluno(a) mencionado(a) acima defendeu seu trabalho final (apresentação oral seguida de arguição) perante uma Banca Examinadora, cujos membros estão listados abaixo. O(A) aluno(a) foi APROVADO(A) pela Banca Examinadora, por unanimidade, em cumprimento ao requisito exigido para obtenção do Título de Doutora em Astrofísica. O trabalho precisa da incorporação das correções sugeridas pela Banca Examinadora e revisão final pelo(s) orientador(es).

Novo Título: "COSMIC CHEMICAL EVOLUTION: MODELING AND COMPARING WITH OBSERVATIONS"

Membros da banca:

Dr. Francisco Jose Jablonski – Presidente – INPE
Dr. Oswaldo Duarte Miranda – Orientador – INPE
Dr. Carlos Alexandre Wuensche de Souza – Orientador – INPE
Dr. José Williams dos Santos Vilas Boas – Membro Interno – INPE
Dr. Reinaldo Ramos de Carvalho – Membro Externo – UNICID
Dra. Karin Silvia Franzoni Fornazier Guimarães – Membro Externo – USP

Documento assinado eletronicamente por **Reinaldo Ramos de Carvalho (E)**, **Usuário Externo**, em 18/10/2022, às 16:31 (horário oficial de Brasília), com fundamento no § 3º do art. 4º do Decreto nº 10.543, de 13 de novembro de 2020.

Documento assinado eletronicamente por **Oswaldo Duarte Miranda**, **Coordenador do Gabinete do Instituto Nacional de Pesquisas Espaciais**, em 18/10/2022, às 17:02 (horário oficial de Brasília), com fundamento no § 3º do art. 4º do Decreto nº 10.543, de 13 de novembro de 2020.

Documento assinado eletronicamente por **José Williams dos Santos Vilas Boas**, **Pesquisador**, em 18/10/2022, às 18:18 (horário oficial de Brasília), com fundamento no § 3º do art. 4º do Decreto nº 10.543, de 13 de novembro de 2020.

Documento assinado eletronicamente por **KARIN SILVIA FRANZONI FORNAZIER GUIMARAES (E)**, **Usuário Externo**, em 19/10/2022, às 07:45 (horário oficial de Brasília), com fundamento no § 3º do art. 4º do Decreto nº 10.543, de 13 de novembro de 2020.

Documento assinado eletronicamente por **Carlos Alexandre Wuensche de Souza**, **Chefe da Divisão de Astrofísica**, em 19/10/2022, às 15:57 (horário oficial de Brasília), com fundamento no § 3º do art. 4º do Decreto nº 10.543, de 13 de novembro de 2020.

Documento assinado eletronicamente por **Francisco Jose Jablonksi**, **Pesquisador**, em 24/10/2022, às 12:13 (horário oficial de Brasília), com fundamento no § 3º do art. 4º do Decreto nº 10.543, de 13 de novembro de 2020.

A autenticidade deste documento pode ser conferida no site https://sei.mcti.gov.br/verifica.html, informando o código verificador **10385397** e o código CRC **FF4FB5BB**.

Referência: Processo nº 01340.007330/2022-51 SEI nº 10385397

ACKNOWLEDGEMENTS

Agradeço aos meus orientadores, Oswaldo e Alex, pelo constante apoio, parceria, aprendizados e por todo conhecimento compartilhado ao longo dos últimos anos.

Aos professores e pesquisadores do INPE e de todas as outras instituições os quais tive o prazer de aprender com e de trocar experiências.

À minha família, em especial aos meus pais, Alexandre e Mirna, pelo apoio e incentivo desde o início da minha carreira, sempre muito parceiros, pacientes e, acima de tudo, por serem sempre minhas maiores inspirações.

Ao meu marido, Antonio, agradeço pela paciência, pela parceria, pelo cuidado constante e por tirar o "melhor de mim" em todos os momentos.

Aos meus amigos e colegas de mestrado e doutorado, Dudu e Rafael, que sempre estiveram próximos, não só nos momentos de conquista, mas também nos momentos mais desafiadores e difíceis.

À minha amiga Alice, pelo carinho, por todo apoio e pela parceria construída nos últimos anos.

Aos meus amigos Marcelo, Cecília e Tabuquine, pelo apoio gigante fornecido sempre (e principalmente nos últimos tempos).

O presente trabalho foi realizado com apoio da Coordenação de Aperfeiçoamento de Pessoal de Nível Superior - Brasil (CAPES) - Código de Financiamento 001.

Obrigada!

ABSTRACT

In order to investigate how chemical elements appear and evolve in the cosmological scenario, we present results from a semi-analytical model developed to understand the evolution of the mean metallicity in the Universe, for several different chemical elements, since the formation of Population III (Pop III) stars until today. In particular, we study the contributions of Pop III and Pop II stars in the cosmic history of the production of O, Fe, Zn, Ni, Si, Mg, Al, C, N, P and S. Our main approach is based in coupling the Cosmic Star Formation Rate (CSFR) with chemical evolution equations for the galactic framework. We present results using the CSFR from (PEREIRA; MIRANDA, 2010) (PM-CSFR), developed self-consistently within the hierarchical structure formation scenario, as well as results using an updated version of the PM-CSFR formalism, where we take into account the dependence of metallicity in the parameters used to generate the CSFR. Calculations start at redshift $z \sim 20$, when Pop III stars first started to die, and go up to the formation of Pop II stars with metallicity $Z = 0.02\ Z_{\odot}$. We compare the results with data from Damped Lyman-α systems (DLAs), Globular Clusters (GCs) and Extremely Metal-Poor stars (EMPs). Our main results find that the CSFR has an important role in the total metal production in the Universe at very early times, reaching a peak right after the formation of the first Pop III stars, showing a subsequent decrease as the Universe becomes more metal-rich and Pop II stars start to form. Models using Pop II stars alone are unable to reproduce observed chemical abundances in the redshift range used in the calculations, demanding stars with physical properties similar to what is expected from Pop III stars, not yet observed, but which present substantially better agreement with observations.

Keywords: Chemical Evolution. Cosmic Abundances. First Stars.

EVOLUÇÃO QUÍMICA CÓSMICA: DESENVOLVENDO MODELOS E COMPARANDO COM OBSERVAÇÕES

RESUMO

Com o objetivo de investigar como os elementos químicos surgem e evoluem no cenário cosmológico, apresentamos resultados de um modelo semi-analítico desenvolvido para entender a evolução da metalicidade média no Universo, para diversos elementos químicos, desde a formação de estrelas de População III (Pop III) até hoje. Em particular, estudamos as contribuições das estrelas Pop III e Pop II na produção de O, Fe, Zn, Ni, Si, Mg, Al, C, N, P e S. Nossa abordagem principal é baseada em acoplar a Taxa Cósmica de Formação Estelar (CSFR) com equações de evolução química para galáxias. Apresentamos resultados usando a CSFR de (PEREIRA; MIRANDA, 2010) (PM-CSFR), desenvolvida de forma autoconsistente dentro do cenário de formação de estrutura hierárquica, bem como resultados usando uma versão atualizada do formalismo PM-CSFR, onde levamos em consideração a dependência da metalicidade nos parâmetros utilizados para gerar a CSFR. As simulações começam em redshift $z \sim 20$, quando as estrelas Pop III começaram a morrer, e vão até a formação de estrelas Pop II com metalicidade $Z = 0,02\ Z_{\odot}$. Comparamos os resultados com dados de sistemas Damped Lyman-α (DLAs), aglomerados globulares (GCs) e estrelas extremamente pobres em metais (EMPs). Nossos principais resultados mostram que a CSFR tem um papel importante na produção total de metais no Universo em altos redshifts, atingindo um pico logo após a formação das primeiras estrelas, e mostrando uma diminuição subsequente à medida que o Universo se torna mais rico em metais e estrelas do Pop II começam a se formar. Os modelos que utilizam apenas estrelas de Pop II são incapazes de reproduzir abundâncias químicas observadas na faixa de redshift [0,6], exigindo estrelas com propriedades físicas semelhantes ao que se espera de estrelas Pop III, ainda não observadas, mas que apresentam substancialmente melhor concordância com as observações.

Palavras-chave: Evolução Química. Abundâncas Cósmicas. Estrelas Primordiais.

LIST OF FIGURES

Page

LIST OF TABLES

Page

CONTENTS

1 INTRODUCTION

> *"The nitrogen in our DNA, the calcium in our teeth, the iron in our blood, the carbon in our apple pies were made in the interiors of collapsing stars. We are made of starstuff."*
>
> — Carl Sagan.

Everything around us is made of chemical elements. The production and distribution of elements in the cosmos is the result of many processes, which started early in the history of the Universe, during the Big Bang, and goes on to the present day, inside the nuclei of stars.

The first event in the Universe which produced chemical elements was the primordial (or Big Bang Nucleosynthesis, BBN), responsible for the synthesis of deuterium, ^{3}He, ^{4}He, and traces of ^{7}Li (OLIVE et al., 2000; PITROU et al., 2018). This event was very fast, taking place during the first 20 minutes of the Universe and sets a paradigm that is widely accepted in the scientific community, once it has been precisely modeled and tested (SMITH et al., 1993; STEIGMAN, 2007; IOCCO et al., 2009; MEISSNER; METSCH, 2022).

A few million years after the BBN, another class of matter was playing an important role: Dark Matter (DM). Between the end of recombination era and redshift ~ 20 (180 Myr ater the Big Bang), the first DM halos decouple from the Universe's expansion, collapsing and virializing (PEREIRA; MIRANDA, 2010). The potential wells of these first halos generate the conditions for the baryonic matter to flow into these structures, which agglomerates to form the First Stars and Galaxies.

Figure 1.1 shows the timeline of some important phases of the Universe, such as the Big Bang, the later formation of DM halos and the birth of the first stars and galaxies.

The emergence of first stars characterized the second event, after the BBN, to be responsible for the production of chemical elements. These first stars, composed of only H and He, are the so-called Population III (Pop III) stars. Despite intense observational efforts, these stars have never been observed, although a few candidates have been proposed (e. g., (KASHIKAWA et al., 2012; SOBRAL et al., 2015; VANZELLA et al., 2020)). Thus, researchers have been joining strengths to build consistent modeling of these stars in the past decades (HEGER; WOOSLEY, 2002; SCHAERER, 2002; CHIEFFI; LIMONGI, 2004; HEGER; WOOSLEY, 2010; TAKAHASHI et al., 2018).

Figure 1.1 - Timeline of the Universe's evolution.

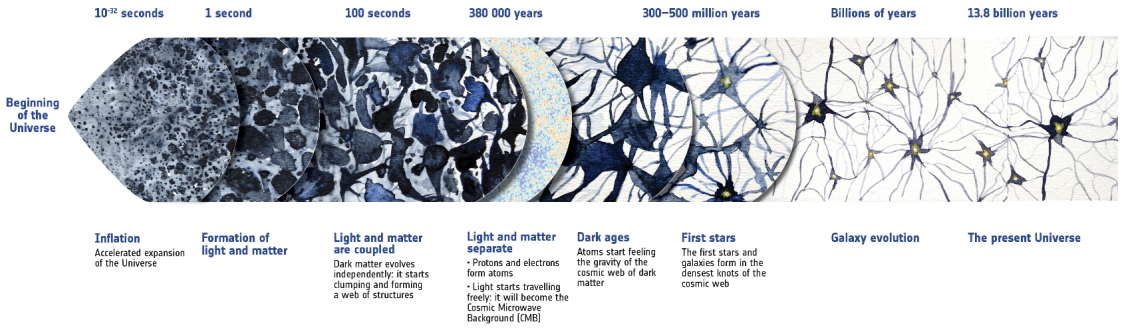

Source: European Space Agency (ESA) (2015).

Due to the lack of metals in the gas, cooling processes, essential for the gas to agglomerate and form stars, were very inefficient (GALLI; PALLA, 2013; HIRANO; YOSHIDA, 2013), indicating that the first stars would have very large masses, between 100 and 200$M_\odot$. Other authors also point to even higher masses, around 500 to 1000$M_\odot$ (see, e.g., Ohkubo et al. (2006)).

In terms of chemical production, the above characteristics indicate they were substantially important. For instance, Pop III stars with masses from 140 to 260 $M_\odot$ produced huge amounts of metals. Also due to their high masses, they quickly ended their lives as Pair-Instability Supernovae (PISNe), injecting large amounts of highly enriched material back into the Interstellar Medium (ISM) and Intergalactic Medium (IGM). Another interesting property of the PISNe is that they leave no remnants behind; instead, they end their lives in a complete disruptive process (HEGER; WOOSLEY, 2002; TAKAHASHI et al., 2018).

Population III stars made the IGM enriched, providing the perfect sites for the formation of a second generation of stars, the Population II stars. With more and more enriched material available, cooling processes started to become more efficient, giving origin to less massive stars with physical proprieties close to those observed today, and also extensively modeled mainly according to their masses and metallicities (CHIEFFI; LIMONGI, 2004; KOBAYASHI, 2005; CAMPBELL; LATTANZIO, 2008; KARAKAS, 2010; DOHERTY et al., 2013; DOHERTY et al., 2014).

These chemical production and enrichment processes remained cyclic: stars are formed, produce chemical elements, die injecting enriched material into the Interstellar Medium (ISM) which gave origin to new, more enriched stars until reaching the abundances observed today. Figure 1.2 illustrates the chemical contributions

from the Big Bang, the First Stars and what we find today through observations.

Figure 1.2 - Image illustrating the main chemical species produced during the Big Bang (top), the main chemical signature from primordial stars (middle) and what we observe today in the Universe (bottom).

Source: Heger ().

Cosmic Chemical Evolution (CCE) is the field of research which accounts for the investigation of all the processes above - from the primordial nucleosynthesis until the observed abundances today. The main goal of CCE is to investigate the origin and evolution of chemical elements along the history of the entire Universe, therefore requiring an ensemble of cosmological theories of structure formation (which will explain the formation of DM halos and the rate of stellar formation) with stellar evolution (nucleosynthetic yields and remnant masses).

In terms of the development of the field, Chemical Evolution models were, however, first developed for the framework of the galaxy (TINSLEY; LARSON, 1978; LARSON et al., 1980; MATTEUCCI, 2016). The level of uncertainty for cosmological parameters at the time prevented the field from advancing to the cosmological framework, but after many advances achieved in the following years, a new window to explore many properties in the cosmology field was opened.

Today, there are several different models which seek to evaluate different aspects related to the galactic and cosmic chemical enrichments, such as the evolution of the mass-metallicity relation (MA et al., 2016; TORREY et al., 2019), the establishment of a critical value for the metallicity of the Universe allowing the transition from Pop III to Pop II stars (BROMM et al., 2001; BROMM; LOEB, 2003; FANG; CEN, 2004; MATTEUCCI; CALURA, 2005; SANTORO; SHULL, 2006; TORNATORE et al., 2007; MAIO et al., 2010; SCHNEIDER, 2010), Hypernovae (HNe) feedback (KOBAYASHI et al., 2007), the role of galactic outflows (DAVÉ; OPPENHEIMER, 2007), the chemical properties of local galaxies based on their formation through the hierarchical model of structure formation (CALURA; MENCI, 2009), the evolution of N abundance in the Universe and the reason for large dispersion in observational data (VANGIONI et al., 2018), the influence of Dark Matter (DM) halos on the gas reservoir available for star formation (LILLY et al., 2013), among other examples of interesting contributions to the study of the Universe through its chemical enrichment.

The models can be generically classified into semi-analytical and hydrodynamical simulations. Nevertheless, there is increasing uncertainty connected to the chemical evolution as we move from local to cosmological scales, which is independent of the analytical or computational modeling. From the small scale represented by nuclear reaction rates and stellar masses to larger, galactic, and cosmological scales, there is a cumulative uncertainty since each scale carries its own sets of considerations and uncertainties.

1.1 Motivation and goals

CCE models mainly discuss general and particular aspects of metallicity evolution ([Z/H] and/or [Fe/H]) in cosmological terms, but several do not detail the contributions to the evolution of single elements. Moreover, comparing observations with high-redshift simulations is a challenge.

We gathered the motivations above to develop a model to investigate the evolution of single element abundances in the Universe. In general terms, our approach is based in coupling a consolidated framework of Galactic Chemical Evolution (GCE) with the cosmological scenario, supported by the theories of large scale structure formation and cosmological star formation rates.

More specifically, we propose a semi-analytical model to investigate the contributions of Pop III and Pop II stars to the cosmological evolution of single elements across the redshift interval $0 \leq z \lesssim 20$, taking into account different perspectives to compare our results with observations in a range of different redshifts.

We start on Chapter 2, introducing and justifying the choices for the cosmological background, which is going to be the basis for the chemical evolution model: we describe the model developed by Pereira and Miranda (2010), and the incorporated changes in the scenario which allow for an adequate coupling of the star formation model with the equations of the chemical evolution of the Universe. We address the adapted cosmological model as CMW along with the text. In addition, the modifications of the model introduced in this work allow a better adjustment of the Cosmic Star Formation Rate (CSFR) to the observational data available up to redshift ~ 10, as well as satisfying all the points studied by Gribel et al. (2017) in their unified model connecting the CSFR with the local star formation.

We also adapted the chemical models developed over the past 40 years for the Galaxy (see, e.g., (TINSLEY; LARSON, 1978; LARSON et al., 1980; MATTEUCCI, 2016)). This adaptation allows us to build an adequate model for the chemical enrichment of the Universe. Implementing chemical yields for stars with masses between 0.85 and 260 $M_\odot$ and metallicities from 0 up to $Z = 0.02\ Z_\odot$ allows us to provide, on Chapter 4, several results, data comparison and discussions about the cosmic evolution of 11 chemical elements: Oxygen (O), Iron (Fe), Zinc (Zn), Nickel (Ni), Silicon (Si), Magnesium (Mg), Aluminum (Al), Carbon (C), Nitrogen (N), Phosphorus (P), and Sulfur (S). We draw the conclusions in Chapter 5.

2 COSMOLOGICAL SCENARIO

As described above, the first dark matter halos decouple from the Universe's expansion, collapsing and virializing, probably between the end of recombination and redshift ~ 20. The potential wells of these first halos generate the conditions for the baryonic matter to flow into these structures, agglomerate, and form the first stars.

The characterization of the cosmological star formation and the consequent chemical enrichment of the Universe is, in this way, connected to the dark matter halo formation within a given mass range and as functions of the redshift.

DM halos drag the baryonic matter into their interiors. We can describe this process through the adaptation of the formalism developed originally by Press and Schechter (1974), which allows to estimate directly the fraction of baryons ($f_{\rm b}$) incorporated into the halos:

$$f_{\rm b}(z) = \frac{\int_{M_{\rm min}}^{M_{\rm max}} f(M,z) M dM}{\int_0^{\infty} f(M,z) M dM}, \tag{2.1}$$

where

$$df(M,z) = \frac{\rho_{\rm m}}{M} \frac{d\ln\sigma^{-1}}{dM} f_{\rm ST}(\sigma) dM \tag{2.2}$$

is the number of DM halos per comoving volume at a given redshift within the mass interval $[M, M+dM]$, and $\rho_{\rm m}$ is the matter density of the Universe.

The halo mass function, $f_{\rm ST}(\sigma)$, proposed by Sheth and Tormen (1999) is:

$$f_{\rm ST}(\sigma) = 0.3222\sqrt{\frac{2a}{\pi}}\frac{\delta_{\rm c}}{\sigma}\exp\left(\frac{-a\delta_{\rm c}^2}{2\sigma^2}\right)\left[1+\left(\frac{\sigma^2}{a\delta_{\rm c}^2}\right)^p\right], \tag{2.3}$$

with $\delta_{\rm c} = 1.686$, $a = 0.707$, $p = 0.3$, and $\sigma(M,z)$ is the variance of the linear density field.

The fact that stars form only in suitably dense structures is parameterized in Equation (2.1) by the threshold mass $M_{\rm min}$. We consider $M_{\rm min} = 10^6 M_{\odot}$ that is the minimum mass for the first star-forming halos to appear in hierarchical models. The upper limit $M_{\rm max}$ can take values up to $\gtrsim 10^{17} M_{\odot}$. This limit is set according to the mass scale of galaxy superclusters (SALVADORI et al., 2007; PEREIRA; MIRANDA, 2010), limiting the scale of the largest structures formed in the present Universe. In any case, the results have shown to be weakly dependent on the upper limit if $M_{\rm max} > 10^{17} M_{\odot}$.

The function $\sigma(M, z)$ in Equation (2.3) can be determined from the power spectrum $P(k)$ smoothed with a spherical top-hat filter function of radius R which, on average, encloses a mass M ($R = [3M/4\pi\rho(z)]^{1/3}$). Thus,

$$\sigma^2(M, z) = \frac{D^2(z)}{2\pi^2} \int_0^\infty k^2 P(k) W^2(k, M) dk, \tag{2.4}$$

where $W(k, M)$ is the top-hat filter in the k-space

$$W(k, M) = \frac{3}{(kR)^3} [\sin(kR) - kR\cos(kR)]. \tag{2.5}$$

The dependence with redshift comes from the growth factor $D(z)$, that is, $\sigma(M, z) = \sigma(M, 0)D(z)$. Here we use the analytical approach for $D(z)$ as derived by Carroll et al. (1992).

The rate at which fluctuations grow on different scales depends on the interplay between self-gravitation, pressure support, and damping processes. All of these processes are part of the power spectrum given by $P(k) \propto k^{n_\mathrm{p}}$ (see, e.g., (GRIBEL et al., 2017) for details).

From these equations, it is possible to determine how halos of different masses decouple from the Universe's expansion and how baryonic matter is gradually incorporated into the center of the virialized halos. Structures more massive than $\sim 10^6 M_\odot$ are formed at later times, as the redshift decreases. Thus, as more halos are formed, more baryonic matter flows into these structures, generating conditions for star formation. This allows us to define the baryon accretion rate as:

$$a_\mathrm{b}(t) = \Omega_{0,\mathrm{b}}\, \rho_\mathrm{c} \left(\frac{dt}{dz}\right)^{-1} \left|\frac{df_\mathrm{b}}{dz}\right|, \tag{2.6}$$

where $\Omega_{0,\mathrm{b}}$ is the baryonic density parameter at $z = 0$, $\rho_\mathrm{c} = 3H_0^2/8\pi G$ is the critical density of the Universe ($H_0 = 100\, h\, \mathrm{km\, s^{-1}\, Mpc^{-1}}$ is the value of the Hubble parameter at the current time), and

$$\frac{dt}{dz} = \frac{1}{H_0(1+z)\sqrt{\Omega_{0,\Lambda} + \Omega_{0,\mathrm{m}}(1+z)^3}}. \tag{2.7}$$

The cosmological framework described through the set of equations presented above

is similar to the one used by different authors (e.g., (DAIGNE et al., 2006); (TAN et al., 2016); (VANGIONI et al., 2018)).

2.1 Star formation scenario

Once we set the cosmological framework, it is possible to compute the CSFR by incorporating the Initial Mass Function (IMF) and the Star Formation Rate (SFR). We explore two scenarios: the first is the original PM CSFR, while the second (hereafter CMW) takes into account different values for the IMF slope, besides taking into account metallicity dependent variables such as the characteristic timescale for star formation and remnant mass.

In particular, the number of stars formed per unit of mass (m), volume (V), and time (t) is given by:

$$\frac{d^3N(m,V,t)}{dmdVdt} = \varphi(m)\,\psi(t), \tag{2.8}$$

where $\psi(t) \propto \rho_{\rm g}^{\alpha}$ corresponds to the SFR ($\rho_{\rm g}$ is the gas density). Note that $\psi(t)$ follows the functional form known as Schmidt's law (SCHMIDT, 1959). On the other hand, the IMF is given by $\varphi(m) \propto m^{-(1+x)}$ and its functional form with $x = 1.35$ is called as Sapeter's IMF (SALPETER, 1959).

2.2 Initial Mass Function

The IMF of the first stars is still an open question. See that the Salpeter IMF favors the formation of low mass stars, and various authors adopted it in their chemical evolution models (see, e.g., (CALURA; MATTEUCCI, 2004; CALURA; MATTEUCCI, 2006; CASEY et al., 2012; SHU et al., 2016; FRASER et al., 2017; VANGIONI et al., 2018)) while some others (see, e.g., (NAKAMURA; UMEMURA, 2001; SCHNEIDER et al., 2006; MA et al., 2017)) also allow for the possibility of a top-heavy or bi-modal IMF.

For the PM CSFR, we consider $x = 1.35$ as the reference value, as described in the original version. However, to identify the influence of the IMF exponent on the chemical enrichment of the Universe, we also considered, for the CMW CSFR, four other values, nominally, 0.85, 1.0, 1.7, and 1.85, allowing the formation of a higher (the first two values) or smaller (the last two values) number of high mass stars when compared to the reference value 1.35. We also used $\alpha = 1$ in agreement with Gribel et al. (2017), which shows that different properties from the star formation

regions in the Galaxy, including the so-called Larson's law, can be well reproduced with $\alpha = 1$.

Therefore, Equation (2.8) describes the number of stars formed within the dark matter halos that aggregate and concentrate baryons in their centers. A fraction of the mass in stars is ejected (through stellar winds and supernovae, for example) and returned to the 'interstellar medium' formed by these structures. The ejected mass fraction is given by:

$$\frac{d^2 M_{\rm ej}}{dV dt} = \int_{m(t)}^{m_{\rm s}} (m - m_r)\psi(t - \tau_m)\varphi(m)dm, \tag{2.9}$$

where $m(t)$ is the stellar mass whose lifetime is equal to t, m_r represents the mass of the remnant. The star formation is taken at the time $(t - \tau_m)$, where τ_m is the lifetime of a star of mass m.

2.3 Remnant mass and time for stellar formation

For the PM CSFR, the remnant mass is metallicity-independent and can be calculated following the prescription bellow (PEREIRA; MIRANDA, 2010):

- For $1\mathrm{M}_\odot < \mathrm{M} \lesssim 8\mathrm{M}_\odot$, remnant is a C-O White dwarf with mass:

$$m_{\rm r} = 0.1156m + 0.4551 \tag{2.10}$$

- If $8\mathrm{M}_\odot < \mathrm{M} \lesssim 10\mathrm{M}_\odot$, the remnant is a O-Ne-Mg white dwarf with mass $m_{\rm r} = 1.35\mathrm{M}_\odot$

- Stars in the interval $10\mathrm{M}_\odot < \mathrm{M} \lesssim 40\mathrm{M}_\odot$ end as neutron stars with $m_{\rm r} = 1.4\mathrm{M}_\odot$

- If $40\mathrm{M}_\odot < \mathrm{M} \lesssim 140\mathrm{M}_\odot$, the remnant is a black hole and

$$m_{\rm r} = m_{He} = \frac{13}{24}(m - 20\mathrm{M}_\odot) \tag{2.11}$$

Notice that stars with $\mathrm{M} < 1\mathrm{M}_\odot$ have lifetimes longer than the age of the Universe and do not contribute to chemical evolution. There is also a high limit mass range where stars collapse directly into black holes, also not contributing to chemical evolution (HEGER; WOOSLEY, 2002).

The time scale for star formation, τ_m, is also metallicity-independent and can be obtained through the relation developed by Copi (1997):

$$\log_{10}(\tau_m) = 10.0 - 3.6 \log_{10}\left(\frac{M}{M_\odot}\right) + \left[\log_{10}\left(\frac{M}{M_\odot}\right)\right]^2 . \tag{2.12}$$

For the CMW CSFR, we take into account metallicity-dependent remnant masses and τ_m. For the remnant mass, we used the results of Spera et al. (2015) to obtain the masses of the stellar remnants (m_r) as functions of the metallicity and the initial stellar masses. The authors obtain their results from SEVN (population-synthesis code) coupled with the PARSEC code for stellar evolution tracks. In particular, we use in this work the fitting formulas presented in Appendix C of Spera et al. (2015).

Concerning the parameter τ_m, the metallicity-dependent formula is given by Raiteri et al. (1996):

$$\log\, \tau_m = a_0(Z) + a_1(Z) \log\left(\frac{M_\star}{M_\odot}\right) + a_2(Z) \left[\log\left(\frac{M_\star}{M_\odot}\right)\right]^2 , \tag{2.13}$$

where τ_m **is expressed in years, and** the metallicity-dependent coefficients are (see (RAITERI et al., 1996) for details):

$$a_0(Z) = 10.13 + 0.07547\, \log Z - 0.008084\, (\log Z)^2, \tag{2.14}$$

$$a_1(Z) = -4.424 - 0.7939\, \log Z - 0.1187\, (\log Z)^2 , \tag{2.15}$$

$$a_2(Z) = 1.262 + 0.3385\, \log Z + 0.05417\, (\log Z)^2, \tag{2.16}$$

and Z is the absolute metallicity.

It is worth stressing that τ_m determined by Equation (2.13) has an excellent agreement when compared to the stellar lifetimes presented in Table 2 of Ekström et al. (2008) for different values of mass and metallicity. In particular, the difference between the results for τ_m is lower than 5% which has little effect on our results.

2.4 Cosmic star formation rate

Following this formalism and combining the previous equations we derive the equation that governs the total gas density $\rho_{\rm g}$ in the halos

$$\dot{\rho}_{\rm g} = -\frac{d^2 M_\star}{dV dt} + \frac{d^2 M_{\rm ej}}{dV dt} + a_{\rm b}(t), \tag{2.17}$$

where the term $a_{\rm b}(t)$ gives for the halos a matter of primordial composition. The system becomes closed without the term $a_{\rm b}(t)$ in Equation (2.17). Thus, this term corresponds to a primordial gas infall in the structures in formation. In other words, it describes the primordial baryonic matter that is captured by the potential wells generated by the halos.

On the other hand, the first term on the right side gives the mass of gas converted to stars per unit of volume and time. By Schmidt's law, we have:

$$\psi(t) = \frac{d^2 M_\star}{dV dt} = k\rho_{\rm g}. \tag{2.18}$$

Note that the term k is the inverse of time-scale for star formation, i.e., $k = 1/\tau_{\rm s}$.

The total gas density can be calculated by numerical integration of the Equation (2.17) providing values for $\rho_{\rm g}(t)$ at each time t or redshift z as long as the $\tau_{\rm s}$ parameter is set.

The initial condition is zero gas density at $z = 20$ for solving Equation (2.17). Moreover, there are some steps for obtaining the correct characterization of the function $\rho_{\rm g}$. They are:

(i) Equation (2.17) explicitly depends on three functions: $\tau_{\rm s}$, $\varphi(m)$, and the (primordial) gas infall $a_{\rm b}(t)$. The last function is determined by the cosmological scenario. The IMF $\varphi(m)$ has the functional form known as Salpeter-IMF (for de PM CSFR) and we explore other values for the x-exponent within the range $[0.85, 1.85]$ as mentioned above for the CMW approach.

(ii) The $\tau_{\rm s}$ parameter is related to CSFR via Schmidt's Law. That is, $\dot{\rho}_\star$ is directly proportional to the gas density and inversely proportional to the characteristic timescale for the conversion of gas in stars. If all the gas entering the system, plus the gas returning to the system through (2.9), is converted into stars, there will be an overabundance of both stars and metals. Thus, $\dot{\rho}_\star$ must also be dependent on a parameter that measures the efficiency ($< \varepsilon_\star >$) in which gas is converted into stars. So the CSFR is:

$$\dot{\rho}_\star(z) =< \varepsilon_\star > \frac{\rho_{\rm g}}{\tau_s}. \tag{2.19}$$

(iii) Once the CSFR is determined, the $a_{\rm b}$ function is fixed by the structure formation scenario, and the IMF is determined by the choice of the x-exponent, then there will be possible to determine the function $\rho_{\rm g}$ by Equation (2.17);

(iv) The previous steps are essential to characterize the total gas density function. The calculation algorithm integrates the differential Equation (14) through the sixth-order Runge-Kutta method. The differential equations for the various chemical elements and total metallicity of the Universe are solved by the same method. As the lifetimes of stars and the masses of stellar remnants also depend on metallicity, the program iterates through the set of equations until the difference between two solutions is less than 10^{-7} within the considered redshift interval. We also run models with tolerance 10^{-10} for checking the accuracy of the solution. The two solutions agree at the 10^{-6} level.

2.5 How to characterize the functions τ_s and $< \varepsilon_\star >$?

For the PM-CSFR, $< \tau_s >= 2Gyr$ and $< \varepsilon_\star >$, the efficiency for star formation, also acts as a normalization factor. The only constraint $< \varepsilon >$ should satisfy is to return at $z = 0$ the value $0.016\, M_\odot\, {\rm yr}^{-1}\, {\rm Mpc}^{-3}$ for the CSFR. It establishes the normalisation according to the value determined by Springel and Hernquist (2003).

For the CMW CSFR, the $< \varepsilon_\star >$ and $< \tau_s >$ functions work together to produce CSFR with the best fit to the observational data.

In particular, the cold gas used to form stars is given by:

$$\rho_{\rm cold}(z) =< \varepsilon_\star > \rho_{\rm g}(z), \tag{2.20}$$

where $< \varepsilon_\star >$ acts as efficiency for star formation, and $\rho_{\rm cold}$ is the gas used for the star formation.

Regarding the characteristic time-scale for star formation, we have:

$$\tau_s(z) = \frac{\rho_{\rm cold}}{\dot{\rho}_\star} \tag{2.21}$$

Equations (2.19), (2.20), and (2.21) are solved together to characterize the CSFR and allow the correct characterization of the dependency of the $< \varepsilon_\star >$ and τ_s functions with the redshift.

For the CMW-CSFR, the constraints associated with these equations are:

(a) produce the best adjustment of the $\dot{\rho}_\star(z)$ curve to the observational data available within the range $[0 - 10]$ in redshift;

(b) normalize $\dot{\rho}_\star$ to return the value $\sim 0.016\, M_\odot\, \mathrm{yr}^{-1}\, \mathrm{Mpc}^{-3}$ at $z = 0$, similar to one determined by Madau and Dickinson (2014);

(c) make the CSFR peak at redshift $z = 2$. This value was chosen so that $\dot{\rho}_\star$ obtained here is in accordance with the peak of the CSFR used by Vangioni et al. (2018) and the one determined by Madau and Dickinson (2014);

(d) produce $< \varepsilon_\star > \sim 0.01 - 0.02$ at $z = 0$. This causes the value $< \varepsilon_\star >$ to be of the order of $\varepsilon_{\mathrm{ff}}$, the so-called star formation rate per free-fall time, inferred for the star-forming regions of the local Universe (see, e.g., (KRUMHOLZ; MCKEE, 2005; GRIBEL et al., 2017));

(e) produce $\tau_s(z = 0) \sim 0.5 - 2.5\,\mathrm{Gyr}$ similar to the value of τ_{dep} as inferred by Schinnerer et al. (2016b) for the local Universe ($z = 0$). Moreover, our models with IMF exponent $x > 1.0$ show good agreement with the fit of Maio et al. (2022) at $z \sim 5$ for the neutral-gas depletion time.

Figure 2.1 shows the PM and CMW CSFRs as a function of redshift and their behavior concerning the observational data.

Figure 2.1 - The solution for $\dot{\rho}_\star(z)$ as originally derived in the PM formalism (purple solid line) and the CMW CSFR plotted for comparison (red solid line). Top: evolution of the CSFR from the local Universe to $z = 20$. Bottom: same as left, but zooming into $0 \leq z \leq 10$, allowing for a better visualization of the two CSFRs within the range of the available observational data. Data used in this figure: IR (Magnelli et al. (2011), Magnelli et al. (2013) - dark red filled diamonds; Gruppioni et al. (2013) - dark blue open squares); UV (Wyder et al. (2005) - purple filled circles; Schiminovich et al. (2005) - blue filled squares; Dahlen et al. (2007) - green open triangles; Reddy and Steidel (2009) - orange filled crosses; Robotham and Driver (2011) - turquoise filled triangles; Cucciati et al. (2012) - yellow crosses; Bouwens et al. (2012a), Bouwens et al. (2012b) - turquoise open diamonds); GRB (Kistler et al. (2009), KISTLER et al. (2013) - pink open circles).

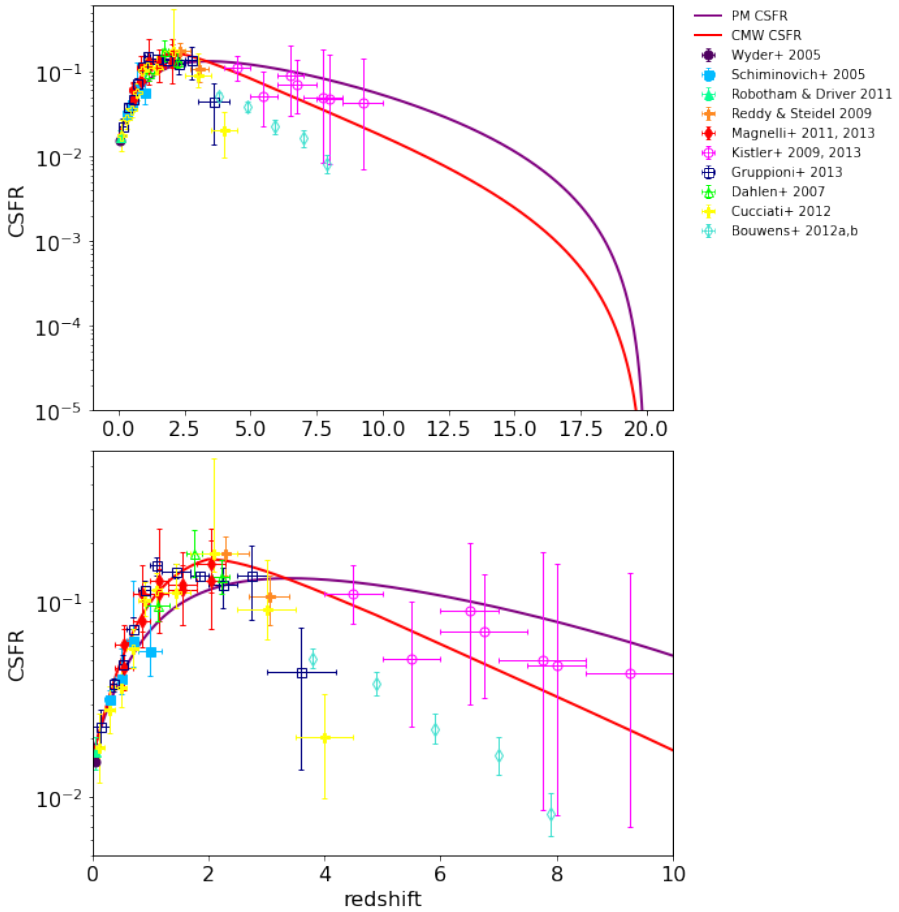

2.5.1 Characteristic time-scale for star formation

In order to address the comparison of τ_s with values from the literature, let us remeber that $\rho_{\rm cold}$ is composed of the sum of two components: molecular gas ($\rho_{\rm H2}$) and atomic gas ($\rho_{\rm HI}$). Equation 2.21 assumes the form:

$$\tau_s(z) = \frac{\rho_{\rm cold}}{\dot{\rho}_\star} = \frac{\rho_{\rm H2}}{\dot{\rho}_\star} + \frac{\rho_{\rm HI}}{\dot{\rho}_\star} \tag{2.22}$$

The present model does not allow for an investigation of each component of $\rho_{\rm cold}$ separately. However, we can compare the behavior of τ_s with the time-scales for the depletion of the different components of the gas, as described by Equation 2.23:

$$\tau_s(z) = \tau_{\rm depl,H2} + \tau_{\rm depl,HI}, \tag{2.23}$$

with $\tau_{\rm depl,H2}$ and $\tau_{\rm depl,HI}$ representing, respectively, the depletion scales for molecular and atomic gases.

As determined by Péroux and Howk (2020), Maio et al. (2022), the corresponding H_2 depletion time follows close to the dynamical time ($\tau_{\rm dyn}$, taken to be 10% of the Hubble time). In Figure 2.2 (left), we present the behavior of the τ_s parameter for different values of the x exponent, compared with the dynamical time. The curve for $\tau_{\rm dyn}$ crosses the curves for τ_s with $x = 0.85$ and $x = 1.0$, *i.e.*, τ_s is smaller than $\tau_{\rm dyn}$ and there would not be enough molecular gas available to be processed into stars near redshift $z \sim 0$. In particular, for $x = 0.85$ this occurs at $z = 0.75$ while for $x = 1.00$ it occurs at $z = 0.38$. Therefore, for both values of x, our model could not follow $\tau_{\rm depl,HII} = \tau_{\rm dyn}$ under these values of z.

In the right panel of Figure 2.2 it is possible to observe the comparison between the results for τ_s with the depletion time-scales for molecular and atomic gas (PÉROUX; HOWK, 2020; MAIO et al., 2022). We can observe that the curves (mainly for $x = 1.35$) are between the colored regions (black and purple) and above t_{dyn}. This means that star formation is maintained by molecular gas and complemented by atomic gas. When the curves for τ_s approach t_{dyn}, a smaller part of neutral gas is used and the greatest part of stellar formation comes com molecular gas, until the moment where τ_s reaches smaller values than t_{dyn}.

Figure 2.2 - Evolution of the characteristic star formation scale (defined as $\tau_s = \rho_{\rm mol}/\dot{\rho}_\star$). Left: Results from the CMW formalism compared with the dynamical time ($\tau_{\rm dyn} \simeq 0.1\, t_{\rm H}$, where $t_{\rm H}$ is the Hubble time) for the redshift interval [0,20]. Right: Same results for τ_s compared with the depletion times for molecular and atomic gas (PÉROUX; HOWK, 2020; MAIO et al., 2022).

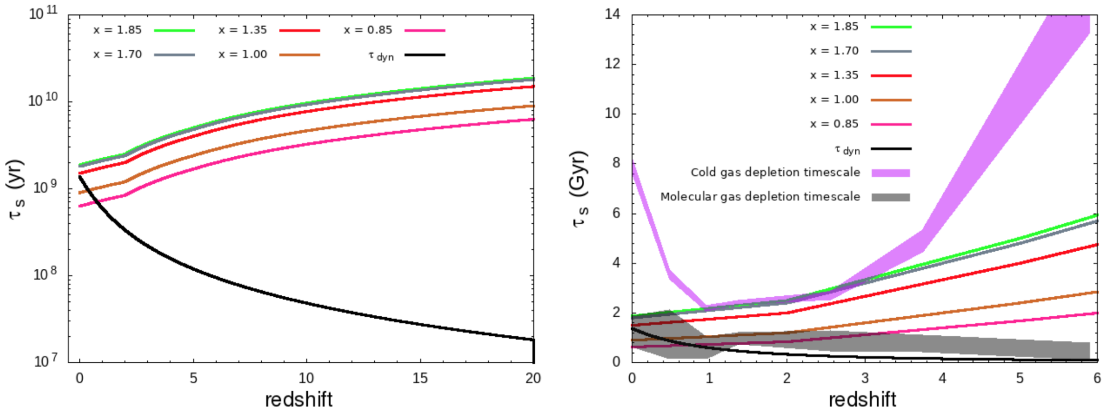

2.5.2 Star formation efficiency

We define the star formation efficiency ($< \varepsilon_\star >$) as:

$$< \varepsilon_\star >= \frac{\rho_{\rm cold}(z)}{\rho_{\rm g}(z)} \tag{2.24}$$

This function represents the fact that not all gas is converted into stars, therefore requiring a factor that we call efficiency. It represents the fraction of the gas that is actually turned into stars at each redshift. This form of efficiency is different from what is commonly presented in the literature[1]. Therefore, in order to allow a comparison with the literature, we can compare our efficiency with the fraction of the gas associated with star formation (f_{gas}) described by the relation (HODGE; CUNHA, 2020):

$$f_{gas} = \frac{M_{gas}}{M_{gas} + M_*} \tag{2.25}$$

where f_{gas} is the molecular gas fraction.

[1]Normally, the Star Formation Efficiency is described by the relation SFE = SFR/M_{gas}, which can be interpreted as the number of stars formed in a certain period.

In Figure 2.3, we present the behaviors of the $< \varepsilon_\star >$ (left), also interpreted as the fraction of gas converted into stars in the CMW formalism and the fraction of gas (f_{gas}) associated with star formation (right) as defined by Equation 2.25, compared with observational data compiled by Hodge and Cunha (2020).

In terms of observational data, Hodge and Cunha (2020) presents a summary of some of the largest studies to parameterise the evolution of the gas fraction as a function of redshift. Scoville et al. (2017), using ALMA observations in a sample of 708 galaxies from $z = 0.3$ to $z = 4.5$ in the COSMOS field (with known SFRs and stellar masses) estimated the total ISM masses. Tacconi et al. (2018) compiled a larger sample of 1444 star-forming galaxies between $z = 0$ and $z = 4$ for which molecular gas estimates were derived using three different methods. Liu et al. (2019) performed the largest study of this kind by combining a dataset of around 700 galaxies (from $z = 0.3$ to $z = 6.0$) from the COSMOS survey and an additional sample of around 1000 CO-observed galaxies from $z = 0$ to $z = 4.0$.

From these studies it is possible to observe that the larger the sample, the harder it is to define scaling relations between the gas mass, SFR and other parameters. Nonetheless, the three studies find that, independently of the sample and methods, the molecular gas mass of main sequence galaxies increases with redshift, *i.e.*, at higher redshifts, a galaxy has more gas available to convert into stars, a compatible behaviour with our simulations.

Also, our results for f_{gas} presented in Figure 2.3 show reasonable agreement with the available observational data described in Hodge and Cunha (2020). Our results for f_{gas} are represented by the mean curves from scaling relations for the gas content, as a function of redshift, of the fits presented by Hodge and Cunha (2020) in their Figure 13b.

In Table 2.1, we summarize the parameters used to obtain the CMW CSFR – $\dot{\rho}_\star(z)$. It depends on the cosmological parameters $\Omega_{\rm m}$, $\Omega_{\rm b}$, Ω_Λ, and the parameters related to the formation of large-scale structures of the Universe (σ_8, $n_{\rm p}$, and $M_{\rm min}$).

Figure 2.3 - Evolution of the fraction of gas converted into stars for different values of the IMF used in this work. Left: evolution of the average star formation efficiency (defined as $< \varepsilon_\star >$) as a function of z. Right: evolution of the fraction of gas associated with star formation (f_{gas}) as described by Hodge and Cunha (2020). Symbols represent observational data as follows: circles (TACCONI et al., 2018), squares (SCOVILLE et al., 2014), diamonds (SCOVILLE et al., 2016), stars (DESSAUGES-ZAVADSKY et al., 2015) and triangles (SCHINNERER et al., 2016a).

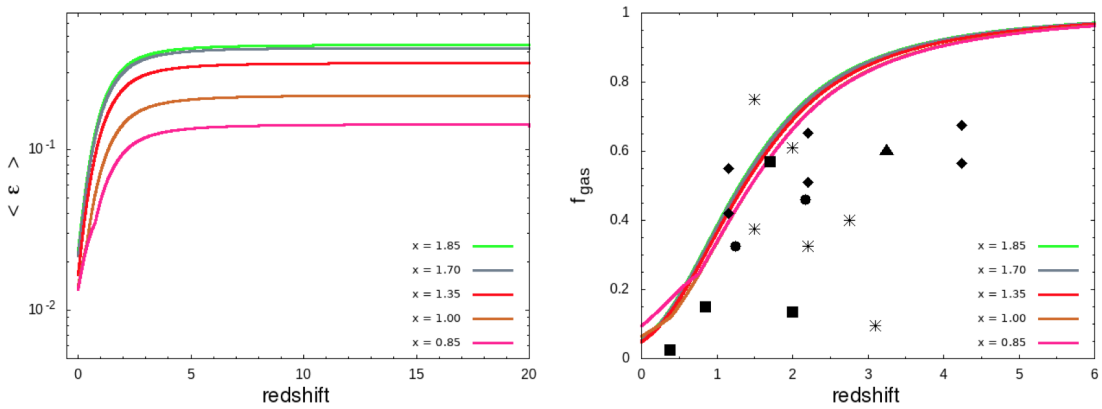

Table 2.1 - Cosmological and structure formation parameters used to obtain the CMW CSFR.

$\Omega_{0,\mathrm{m}}$	$\Omega_{0,\mathrm{b}}$	$\Omega_{0,\Lambda}$	h	z_i	σ_8	n_p	$M_\mathrm{min}(M_\odot)$
0.279	0.0463	0.721	0.7	20	0.84	0.967	10^6

Note. Ω_m corresponds to the total matter (baryonic plus dark matter) density parameter; Ω_b is the baryonic density parameter; Ω_Λ is the density parameter associated with dark energy (cosmological constant); h is the Hubble constant written as $H_0 = 100\,h\,\mathrm{km\,s^{-1}\,Mpc^{-1}}$; z_i is the redshift at which star formation begins; σ_8 is the normalization of the power spectrum, in other words $\sigma(M, 0)$; n_p is the spectral index of the power spectrum; M_min corresponds to the lowest mass a dark matter halo must have to detach from the expansion of the Universe, to collapse and to virialize (it is approximately equal to the Jeans mass at recombination).

Although our model is semi-analytical, by adding the redshift dependency to the functions $< \varepsilon_\star >$ and τ_s it becomes possible to obtain $\dot{\rho}_\star(z)$ with an adequate behavior within the redshift range where CSFR data exists. In addition, the way we build $< \varepsilon_\star >$ and τ_s with the constraints that these functions must satisfy at $z = 0$, shows good agreement with the observational data as described in the last subsections.

3 CHEMICAL EVOLUTION SCENARIO

In order to build a chemical evolution model some basic ingredients are required: the initial conditions and stellar formation rate (already accounted by the cosmological scenario), chemical evolution equations (which are going to account for the fate of available enriched and non enriched gas) and stellar chemical yields (which are going to provide the amount of chemical elements each star is going to produce.)

3.1 Formalism

The first chemical evolution models were developed for the framework of the Galaxy by Tinsley and Larson (1978), Larson et al. (1980) and later by Matteucci (2001). Their simple model of chemical evolution considers a closed-box evolving system with no inflows or outflows. Also, the IMF is constant in time, the chemical composition of the gas is primordial, and the mixing between the chemical products ejected by stars and the ISM is instantaneous.

We can adapt these concepts, which are the basis of the chemical evolution models of the Galaxy, straightforwardly. The main difference is that in the cosmological scenario, the halos continuously incorporate baryons (primordial gas) from the ambient (Universe). This is described by the function $a_{\rm b}(t)$.

Once inside the halos, the gas is removed from the system to form stars at time $t - \tau_m$. This is described using the CSFR $\dot{\rho}_\star(t - \tau_m)$. Later, the gas returns to the system, at time t, when the stars die. A certain fraction of the gas used for the star formation in $t - \tau_m$ will be retained in the remnant population m_r that forms in the time t. A new generation of stars will be formed in the instant t, removing gas from the system and this processes is repeated in a cycle of continuous gas capture and chemical enrichment of the environment.

To determine the chemical enrichment of a given i-element, in addition to the functions $\dot{\rho}_\star$ and $a_{\rm b}$, we need to know how much mass of the i-element is returned when the star of mass m dies. This is described by the parameter $P_{Z_{\rm i}m}$ that provides the "stellar yield" of the i-element.

Once all of these functions and parameters are characterized, we can write a differential equation for the mass density of the i-element as:

$$\frac{d\rho_{\rm gi}}{dt} = \int_{m(t)}^{m_{\rm s}} [(m - m_r) Z_{\rm i}(t - \tau_m) + P_{Z_{\rm i}m}]\, \dot{\rho}_\star(t - \tau_m)\varphi(m)dm - Z_{\rm i}\dot{\rho}_\star(t), \quad (3.1)$$

where the term $(m-m_r)\, Z_{\rm i}(t-\tau_m)$ accounts for the amount of i-element incorporated when the star was born and which later returns to the ISM (see that $m_r\, Z_{\rm i}(t-\tau_m)$ is the part of the i-element retained into the remnant). The term $Z_{\rm i} = \rho_{\rm gi}/\rho_{\rm g}$ brings the function $a_{\rm b}(t)$ into the chemical equation. The $P_{Z_{\rm i}m}$ parameter is the mass produced of the i-element by a star of mass m. The term $Z_{\rm i}\dot{\rho}_\star(t)$ takes into account the removal of part of the i-element to form a new star generation [1].

Through the time integration of Equation (3.1), we obtain the mass density $\rho_{\rm gi}$ of the i-element present in the gas contained within the halos. This allows us to determine quantities such as, e.g., [X$_i$/H] as a function of redshift (or time) and to compare the results of our model with different observational data. Note that Equation (3.1) incorporates all the physics and constraints discussed in the previous Sections.

In order to incorporate the contributions of particular stars, depending on their masses and metallicities, we selected stellar yields. These chemical yields are used to determine the elements that were ejected into the ISM at a given time by a star of a given mass and metallicity. They are calculated through detailed nucleosynthesis computational simulations, considering the main reactions that happen inside the stars. We consider the first stars to be zero metallicity stars (Pop III); the subsequent more enriched Pop II stars are chosen within a range of different masses and metallicities. Tables 3.1 and 3.2 describe the stellar mass and metallicity ranges from where the chemical yields were chosen.

Table 3.1 - Masses selected for Pop III chemical yields.

Model	CL08	HW10	HW02
Metallicity ($Z_\odot$)		Mass ($M_\odot$)	
0	0.85 - 3.0	10 - 100	140 - 260

Note. CL08: Campbell and Lattanzio (2008); HW10: Heger and Woosley (2010); HW02:Heger and Woosley (2002)

[1] A simplified version of this chemical model, within the Pereira and Miranda (2010) scenario, was developed by Vitti (2012). Her model estimated the evolution of O and Zn from the Pop III branch developed by Heger and Woosley (2002).

Table 3.2 - Masses and metallicities selected for Pop II chemical yields.

Model	K10	D13	D14	CL04
Metallicity ($Z_\odot$)		Mass ($M_\odot$)		
10^{-6}	-	-	-	13 - 35
10^{-4}	1 - 6	-	6.5 - 9.0	13 - 35
10^{-3}	-	-	6.5 - 9.0	13 - 35
4×10^{-3}	1 - 6	6.5 - 9.0	-	-
6×10^{-3}	-	-	-	13 - 35
8×10^{-3}	1 - 6	6.5 - 9.0	-	-
2×10^{-2}	1 - 6	6.5 - 9.0	-	13 - 35

Note. K10:Karakas (2010); D13: Doherty et al. (2013); D14: Doherty et al. (2014); CL04: Chieffi and Limongi (2004).

Properly modeling chemical yields for Pop III stars is a challenging and complex task. For the range where they become PISNe, we chose to work with results from Heger and Woosley (2002) which are compatible with recent chemical yields calculated by Takahashi et al. (2018) (hereafter TK18), which takes into account rotating progenitors. The two models (HW02 and TK18) show no significant difference in the explosive yields for the elements chosen here, except for the large production of N in TK18 non-magnetic rotating models. The N behavior can be better understood on a detailed recently developed model for the cosmological evolution of this element (VANGIONI et al., 2018).

For Pop II, samples were chosen according to the best combination of mass and metallicity ranges and also according to the stellar evolution models and parameters used to produce each sample; Karakas (2010), Doherty et al. (2013), Doherty et al. (2014) used the MONSTAR code for stellar evolution (FROST; LATTANZIO, 1996), OPAL opacities (IGLESIAS; ROGERS, 1996) and compatible mass loss models (REIMERS, 1975; VASSILIADIS; WOOD, 1993; BLOECKER, 1995).

3.2 Constructing the models

We explore two scenarios. The first (model A) considers the chemical evolution of the Universe starting with the Pop III (masses and yields as shown in Table 3.1) stars. Once the metallicity of the Universe reaches $Z = 10^{-6} Z_\odot$, no more Pop III stars can be formed. As a consequence, the Pop II stellar branch with $Z = 10^{-6} Z_\odot$ is born and evolves (masses and yields as shown in Table 3.2). This second step finishes when the metallicity of the Universe reaches $Z = 10^{-4} Z_\odot$ and, as a consequence, no more Pop II stars can be formed within the branch $Z = 10^{-6} Z_\odot$. This process

repeats every time the metallicity of the Universe crosses the limits indicated in Tables 3.1 and 3.2. Note that the stars within the low metallicity branches cannot form anymore as a consequence of the increase in the chemical enrichment of the Universe. However, stars with low mass born within the lowest metal branch can still be alive now. Thus, they can co-exist with stars of much higher metallicity during part of their lives. We explore this scenario for the PM and CWM CSFR in relation to the total metallicity of the Universe.

For the second scenario (model B), we consider the chemical evolution only with Pop II stars, for the CMW CSFR. In this case, the 'first-stars generation' ($Z = 0$) of the Universe was composed of stars with masses and chemical yields similar to the Pop II stars of the branch $Z = 10^{-6} Z_{\odot}$ as those studied by Chieffi and Limongi (2004). The following steps are similar to those described for model A. Both scenarios are generated with the CSFR described in 2.1. We describe the evolution of models A and B in 3.2.1 and sec. 3.2.2.

3.2.1 Model A

Model A runs the following steps for the entire calculation: first, the total metallicity of the Universe ($Z_{\rm total}$) is used as 'a guide' for the chemical yields of the different classes (or branches) presented in Tables 3.1 and 3.2. Assuming that the first stars, formed from pristine (H and He only) gas, started to die and enrich the ISM at redshift $z = 20$, $Z_{\rm total}$ provides values for the evolution of the production of all elements heavier than He for the entire redshift interval. This parameter is then used as a 'switch' between different metallicities, removing the chemical yields of a given metallicity and successively introducing those of the higher metallicity classes according to Tables 3.1 and 3.2 and as discussed above.

Abundances of individual chemical elements are then computed for the entire redshift range. $Z_{\rm total}$ starts at zero, producing Pop III stars. The higher mass ones ($\sim 260\, M_{\odot}$) start dying first, throwing metals into the ISM and enriching the medium around them. Pop III stars continue to die and enrich the ISM until the medium reaches $10^{-6} Z_{\odot}$. At that point, new Pop III stars *stop* forming. Note that Pop III stars with masses $\lesssim 0.9 M_{\odot}$ have longer lifetimes and should be still in their Main Sequence phase today, just following the increase of the total metallicity of the Universe, and will participate in subsequent steps of the enrichment of the Universe when they leave the Main Sequence, along with the contribution of new, higher-metallicity stars formed later then that population, at much lower redshifts.

Once the metallicity of the ISM/IGM reaches $10^{-6}Z_{\odot}$, new stars with this metallicity signature start being formed. As they die, the model starts processing the yields from this class of stars, and the same process repeats. The metallicity from the medium increases as the higher mass stars die first, while lower mass stars live longer. Even with stars with higher metallicity ($10^{-4}Z_{\odot}$, for example) starting to form, the lower mass ones will continue their lives unaffected by the external increase of metallicity.

The process continues as the Universe progresses towards the present metallicity, as described in Tables 3.1 and 3.2. It is important to emphasize that each metallicity class has its own "stellar population clock" triggered when the Universe's metallicity crosses the various thresholds indicated in Tables 3.1 and 3.2. Thus, at certain intervals of time, the chemical enrichment of the Universe takes place by the joint action of stars of different metallicity classes.

3.2.2 Model B

Model B uses only Pop II yields. The chemical enrichment of the Universe starts from $Z_{\rm total} = 0$ at redshift 20. For the second Model, we consider that the stellar branch $Z = 10^{-6}Z_{\odot}$ also represents the metal-free stars. Thus, chemical enrichment will occur through this class (or branch) until reaching $Z = 10^{-4}$, when then the next metallicity class (with $Z = 10^{-3}Z_{\odot}$) will assume the control of chemical enrichment. The following branches will take the 'enrichment command' at the points indicated in Table 3.2.

Chemical elements analyzed in this work were selected considering the availability of chemical yields in the literature and observational data available for chemical abundances in Damped Lyman-α Systems and globular clusters, as described in the next Section.

Since there is no clear agreement in the literature on how feedback parameters should be used and what their effect in the evolutionary path in the cosmological context is, we do not take its contribution into account in our calculations. Its contribution to the final result should be negligible, compared to the total value of baryons inside collapsed structures and, therefore, should not affect the general analysis (DAIGNE et al., 2004). We also work with an instantaneous mixing approximation.

4 RESULTS AND DISCUSSION

In this Chapter we present and discuss a series of results regarding the evolution of chemical elements (total metallicity and single elements) in the frameworks described in the previous Chapters.

4.1 The role of the CSFR

We compare the evolution of [Ztot/H] along with redshift considering the two CSFRs described before: the original PM approach and the updated version presented in this work, the CMW CSFR (for x=1.35, same as the original PM model). We compare the results with observation from Damped Lyman-alpha systems from Cia et al. (2018).

The model using the CMW CSFR presents a better fit with observational data than the one using the PM CSFR.

As mentioned above, the the CMW formalism (CSFR and chemical evolution scenario) takes into account the dependence on metallicity of several parameters such as the lifetime of the stars and the remnant mass (which are calculated as functions of the metallicity), while the PM formalism uses metallicity-independent parameters. Also, the PM formalism takes a constant value for τ_s while the CMW formalism also takes into account the time scale for stellar formation as a function of metallicity (and as a consequence, a function of redshift). This update of the CMW scenario allows for a more complete representation of the phenomena in question.

Furthermore, the fact that the updated CMW formalism presents a better fit with observational data shows us that these parameters have a very important role in the physical processes concerning the rate of star formation in the chemical evolution scenario.

These results can be observed in Figure 4.1.

Once the updated model (CMW) presented in this work is, therefore, more accurate for this scenario, we will explore the following results within this framework.

Figure 4.1 - Top: The total metallicity of the universe along redshift for two difeerent CSFRs: The PM formalism (purple solid line) and the CMW formalism (green dashed line). Bottom: Same as the upper image, but in a smaller redshift range in order to compare with DLA abundances.

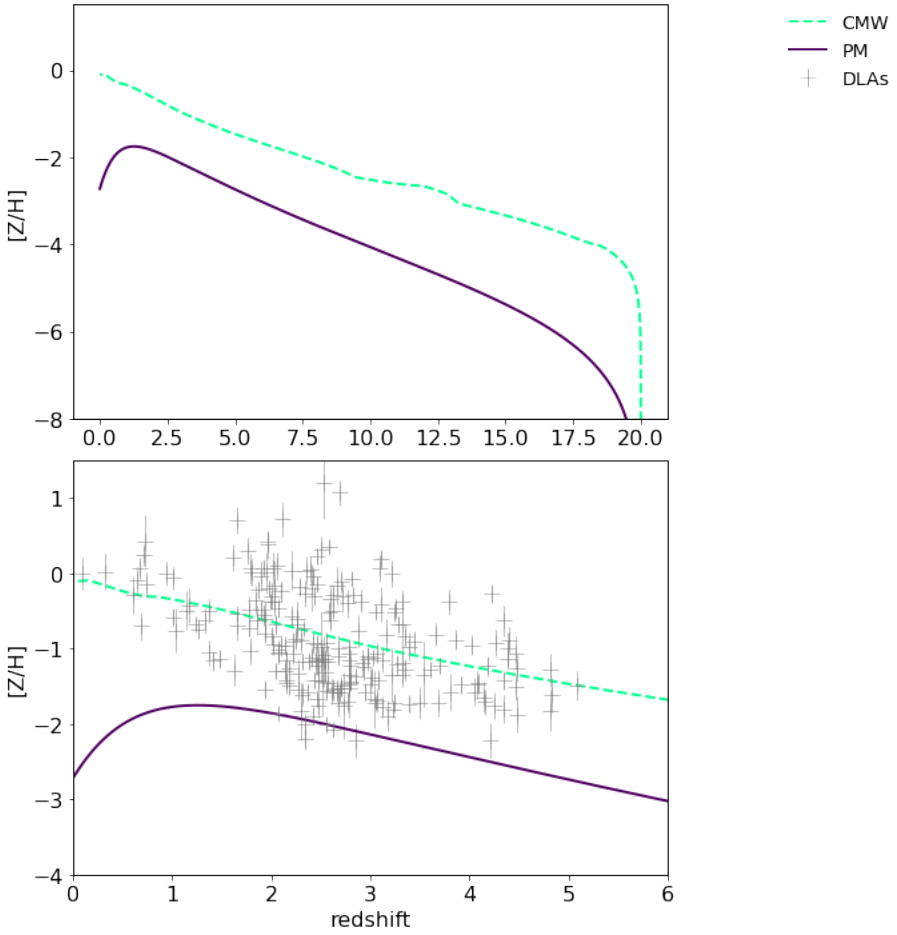

4.2 Evolution of [Z/H] and [Fe/H]

The results from models A and B for $[Z_{\text{total}}/\text{H}]$ are obtained from the CMW-CSFR for five different IMF values and integrated for all ranges from Pop III to Pop II, for model A, and for all ranges of Pop II, for model B. We take into account the progressive enrichment of the Universe and consequently the transition between Pop III and the next more metal-rich Pop II generations until $Z = 0.02\ Z_{\odot}$. The results are presented in Figure 4.2.

Figure 4.2 - Evolution of total metallicity for different values of x in the CMW formalism. Top: Model A (Pop II + Pop III). Bottom: Model B (only Pop II). Colors represent different values of x for the IMF.

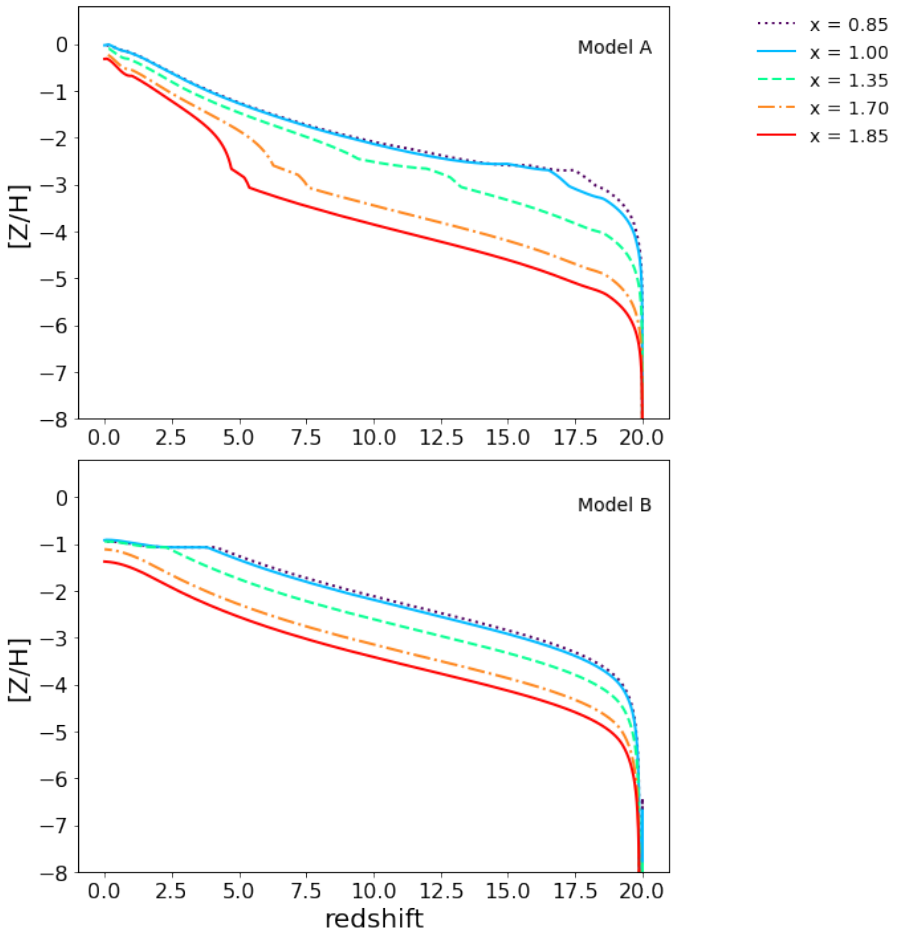

For model A, at redshift $z = 20$, the first stars formed from metal-free gas start to die, and the chemical enrichment is very fast. For $x = 0.85$ and $x = 1.00$, the pristine Universe leaves from $Z = 0$ to reach $Z = 10^{-6} Z_{\odot}$ in less than $\sim 10^5$ yr, given the higher number of high mass stars that would form in this scenario. For $x = 1.70$, the same metallicity is reached ~ 2 Myr after the death of the first Pop III star, while for $x = 1.85$, it would take ~ 4.6 Myr for the same process to occur. The mean behavior is described by $x = 1.35$, where the Universe would reach $Z = 10^{-6} Z_{\odot}$ in 2.8×10^5 yr. For model B, the same process takes from ~ 2 Myr up to 4.5 Myr, depending on the IMF.

This rapid chemical enrichment in the initial phase can be explained by the metal production of Pop III−PISNe, which characterizes a chemical 'flood' in the high redshift Universe, in the case of model A. For model B, the chemical enrichment

occurs mainly through stars with masses $\sim 30 - 35 M_{\odot}$, and the condition $Z = 10^{-6} Z_{\odot}$ is reached eight times slower than when considering higher mass, Pop III stars.

During the Pop III era, all elements are mainly produced by PISNe (with exception of Nitrogen, which will be discussed in the next Sections). According to Abia et al. (2001), the metallicity observed at high redshifts can be easily obtained from stellar pregalactic (Pop III) nucleosynthesis by postulating that only $\sim 10^{-2}$ of the total pristine gas is converted into stars. Considering that the star formation efficiency of the CMW scenario is ~ 0.3 in the redshift range $[5 - 20]$, which is ~ 30 times larger than the value estimated by Abia et al. (2001), we verify that adding Pop III stars in the CMW scenario for the CSFR quickly "floods" the primordial Universe with metals.

Other evidence that PISNe is very efficient in enriching the interstellar medium comes from the work of Matteucci and Calura (2005) where they show that only 110 to 115 PISNe would be needed to enrich a cubic megaparsec of the IGM to $Z = 10^{-4} Z_{\odot}$ (with the index of the IMF varying between 1.35 and 0.5).

In order to adequately address the question of the rapid contamination of the early Universe, we propose comparing the results with abundances from old Extremely Metal-poor Stars (EMPs) and Globular Clusters (GCs). EMPs and GCs (with ages close to the age of the Universe) present an opportunity to explore the chemical and physical conditions of the earliest star-forming environments in the Universe (DOTTER et al., 2011; FREBEL; NORRIS, 2015) *i.e.*, they should present a metallicity value very similar to the Universe's mean metallicity at the time they were formed.

Figure 4.3 shows the comparison between Models A and B with EMPs stars: HE 1523-0901 (FREBEL et al., 2007), HD 140283 (BOND et al., 2013), BD +17°3248 (COWAN et al., 2002) and CS31082-0018 (CAYREL et al., 2001).

The problems in using EMP stars are the large errors associated with age determination on these types of very old stars. Despite the large errors, we have been able to the match the values for [Fe/H] from our model with EMP stars.

Figure 4.3 - Comparison of [Ztot/H] from the model with Extremely Metal-Poor Stars. The purple stars refer to EMP stars: HE 1523-0901 (FREBEL et al., 2007), HD 140283 (BOND et al., 2013), BD +17°3248 (COWAN et al., 2002) and CS31082-0018 (CAYREL et al., 2001).

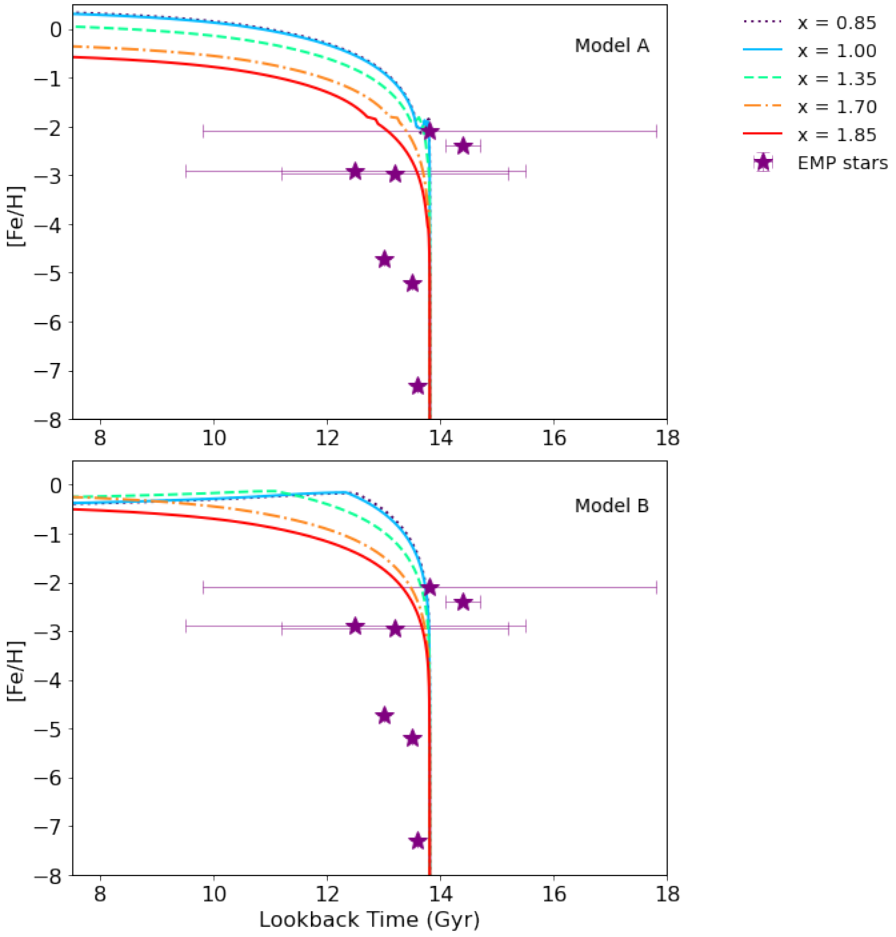

Figure 4.4 - Comparison between models A (left) and B (right) with data from Globular Clusters from (FREBEL et al., 2007; BOND et al., 2013; COWAN et al., 2002; CAYREL et al., 2001; DOTTER et al., 2011; WAGNER-KAISER et al., 2017).

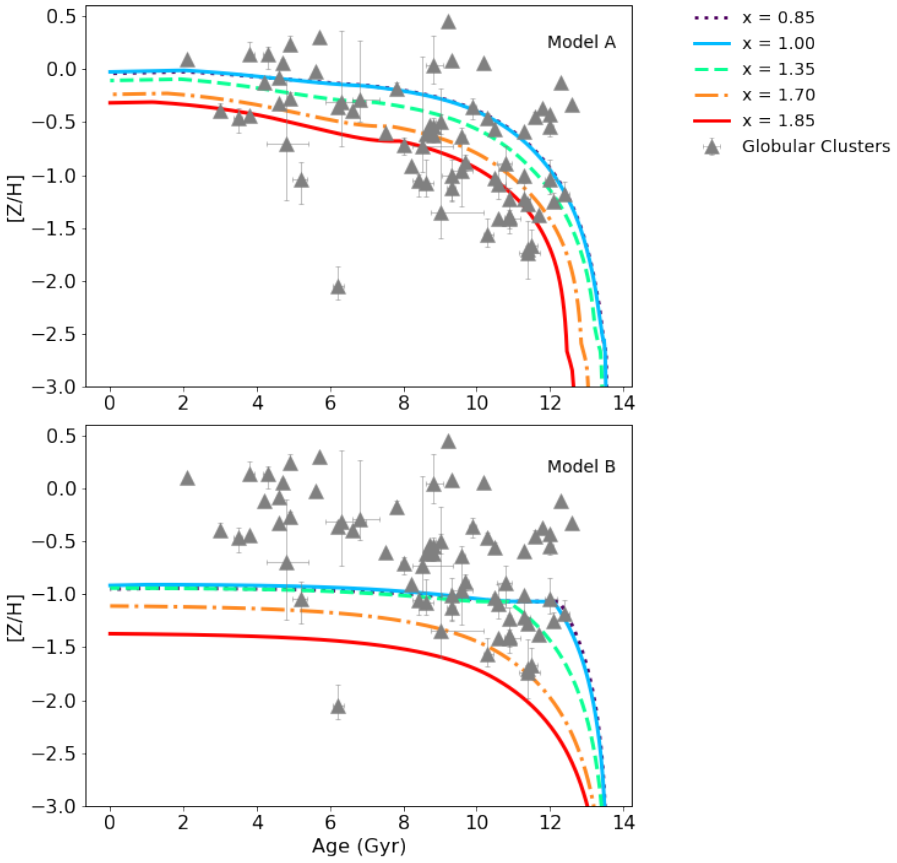

Globular clusters (GCs), on the other hand, provide an integrated age and metallicity for the entire group of stars. Analysis of old GCs data can provide information about age and metallicity for the entire cluster, allowing better estimations than isolated, metal-poor stars, for example. Figure 4.4 shows the behavior of Z_{total} for the two models compared with observations from GCs. Model A accounts for the majority of observations, regardless of the IMF, while model B is unable to fit the metal abundances for Z_{total} even for the lower values of x. Although Pop II with low metallicity and large masses do indeed play an essential role in the first steps of cosmic enrichment, it is clear that their contribution alone is insufficient to allow the ISM to maintain efficient star formation in order to reach the observed metal abundances along the cosmic history.

Figure 4.5 - Comparison of models A (left) and B (right) with data from dust-corrected DLAs (grey crosses) from Cia et al. (2018). We include an α-enhancement correction, with $[Z/\mathrm{H}] = [\mathrm{Fe/H}] + 0.3$ dex as suggested by Rafelski et al. (2012).

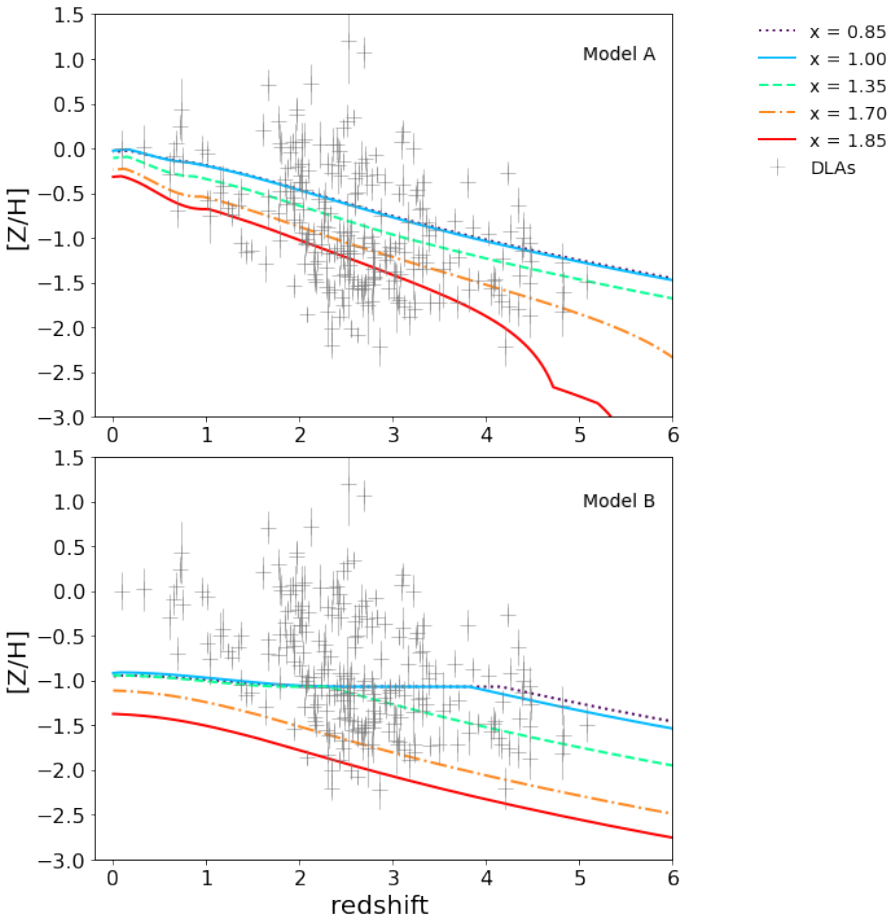

Another analysis is performed for the interval $z = [0 - 6]$, where we compare the results with dust-corrected abundances from Damped Lyman-alpha Systems (DLAs) (Figure 4.5). DLAs provide the most accurate measurements of chemical abundances on the gas-phase for the high-redshift Universe (WOLFE et al., 2005), and abundances can be determined with errors ≤ 0.1 dex (VLADILO, 2002). DLAs are also the perfect site for the initial stages of gas cooling and star formation (MAIO; TESCARI, 2015); they dominate the neutral gas content of the Universe in the redshift interval $z = [0 - 5]$ and therefore are the most crucial neutral gas reservoir for star formation.

In this redshift interval, regardless of the observations, we expect to see an increase of $[Z_{\mathrm{total}}/\mathrm{H}]$ with decreasing redshift, with the total metallicity reaching values close to $\sim$ 0 (solar) near redshift z $\sim$ 0. This behavior is consistent with observations presented in similar contexts (FYNBO et al., 2006; DAVÉ; OPPENHEIMER, 2007;

KOBAYASHI et al., 2007; ROLLINDE et al., 2009; VANGIONI et al., 2018). Also, as pointed out by Calura and Matteucci (2004), main metal production in spirals and irregulars is always increasing with time.

It is possible to observe that, for model B, for $x < 1.35$ the abundances reach a maximum at redshift $z \sim 4$ and start decreasing towards $z = 0$, while for $x \geq 1.35$, metallicities tend to rise with decreasing redshift. Nevertheless, all the B Models remain between -1.0 and -1.5 dex lower than the expected value for $z \sim 0$.

On the other hand, when taking into account Pop III stars (model A), metallicities increase continuously as redshift approaches to $z \sim 0$. For $x = 0.85$, $x = 1.00$ and $x = 1.35$, models reach $[Z_{\text{total}}/\text{H}]$ close to 0, as expected, while for $x = 1.70$ and 1.85, the total metallicity is underestimated by approximately 0.25 to 0.30 dex.

When comparing results with DLA observations, there are two main problems that are relevant to the interpretation of our results. The first is the high dispersion between points relative to the same (or very close) redshift. There is a variety of models investigating dispersion in DLAs (see, for example, Dvorkin et al. (2015)), and some authors agree that it happens due to peculiar nucleosynthetic signatures from each system and also due to different star formation histories (CENTURION et al., 1998; PETTINI et al., 2000; DESSAUGES-ZAVADSKY et al., 2002; CIA et al., 2016), what leads to the production of different amounts of each chemical element.

According to Cia et al. (2016), regardless of the star formation history, the availability of refractory metals in the ISM is a crucial driver of dust production, and DLA galaxies may have a wide range of star formation histories, which in principle are also different from those of the Galaxy (CIA et al., 2016). Therefore, we plot the mean value between the models with different IMFs, suggesting that results for $x = 0.85$ represent the upper limit (due to the favorable formation of high mass stars in this Model) and $x = 1.85$ as the lower limit (due to the favorable formation of lower mass stars).

The second problem in comparing results with DLA observations relates to dust depletion. Some chemical elements react with different species, forming molecular compounds which can get trapped on the surface of dust grains and cannot be detected by the observations of abundances in the gas phase, i.e., abundances would look lower than their actual values. The majority of the results indicate that the behavior of dust depletion on DLAs is complex and varies from system to system (VLADILO et al., 2011; CIA et al., 2016; CIA et al., 2018).

Therefore, we compare our results with dust-corrected DLA metallicities from (CIA et al., 2018). The author shows that when including dust corrections, the average DLA metallicities are between 0.4 and 0.5 dex higher than without corrections. Once the author provides values for [Fe/H], we include an α-enhancement correction, with $[Z/\mathrm{H}] = [\mathrm{Fe/H}] + 0.3$ dex as suggested by Rafelski et al. (2012).

To better estimate the difference between the models and DLA observations, we check for the independence of the samples (chi-squared test with $p = 0.98$), fit a linear relation to the data, and compare with the mean of Models A and B In Figure 4.6.

Figure 4.6 - Results for [Z/H] for the mean of Models A and B compared with a linear fit from DLA observations from Cia et al. (2018).

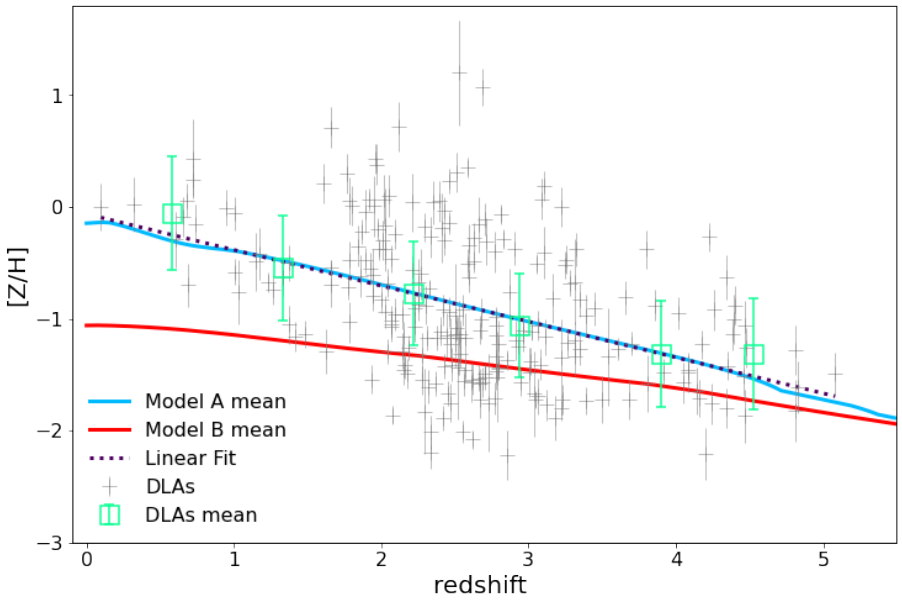

We point out that a linear fit to the data might not be a good description of the data, especially at low and high redshifts, as suggested by Cia et al. (2018). However, the proper accordance between the linear fit and model A suggests that the mean rate of cosmic enrichment might be well represented by our model A.

Some biases could be discussed in this context, such as the fitting of DLA data and the α-enhancement correction. Additionally, chemical yields play a critical role in chemical evolution models, and the inclusion of Pop II yields of lower masses (complementing the models selected in Table 3.2) could provide further enlightenment on the implications of different sets of yields on the behavior of the chemical

abundances towards $z = 0$.

Either way, we reinforce that we aim to demonstrate that Pop III stars are required to represent mean cosmic abundances, which can be straightforwardly observed in Figs 4.4 and 4.6. The impact of different depletion-corrected methodologies, fitting of the data, and the use of different chemical yields should be addressed in detail in the future.

4.3 Evolution of single elements

In this section, we present the cosmic chemical evolution for 11 chemical elements for models A and B, compared with data from DLAs taken from the literature (Figure 4.7), and briefly discuss the main subjects regarding each of the elements. Observational data for other elements are not dust-corrected due to the lack of sufficient data points with enough information for correction (such as [Zn/Fe] or [Si/Fe]).

Figure 4.7 - Chemical evolution for O, Fe, Zn, Ni, Si, Mg, Al, C, N, P, and S since the first stars started to die ($z = 20$) until $z = 0$. The model 'A' starts with zero-metallicity stars, and as the Universe gets enriched, subsequent Pop II stars with increasing metallicity start to appear, until reaching $Z = 2 \times 10^{-2} Z_{\odot}$, according to the model described in 3.2. It is possible to observe the chemical avalanche in the early Universe given by the high production of metals from Pop III stars. As discussed in the text, the model 'B' considers only Pop II stars.

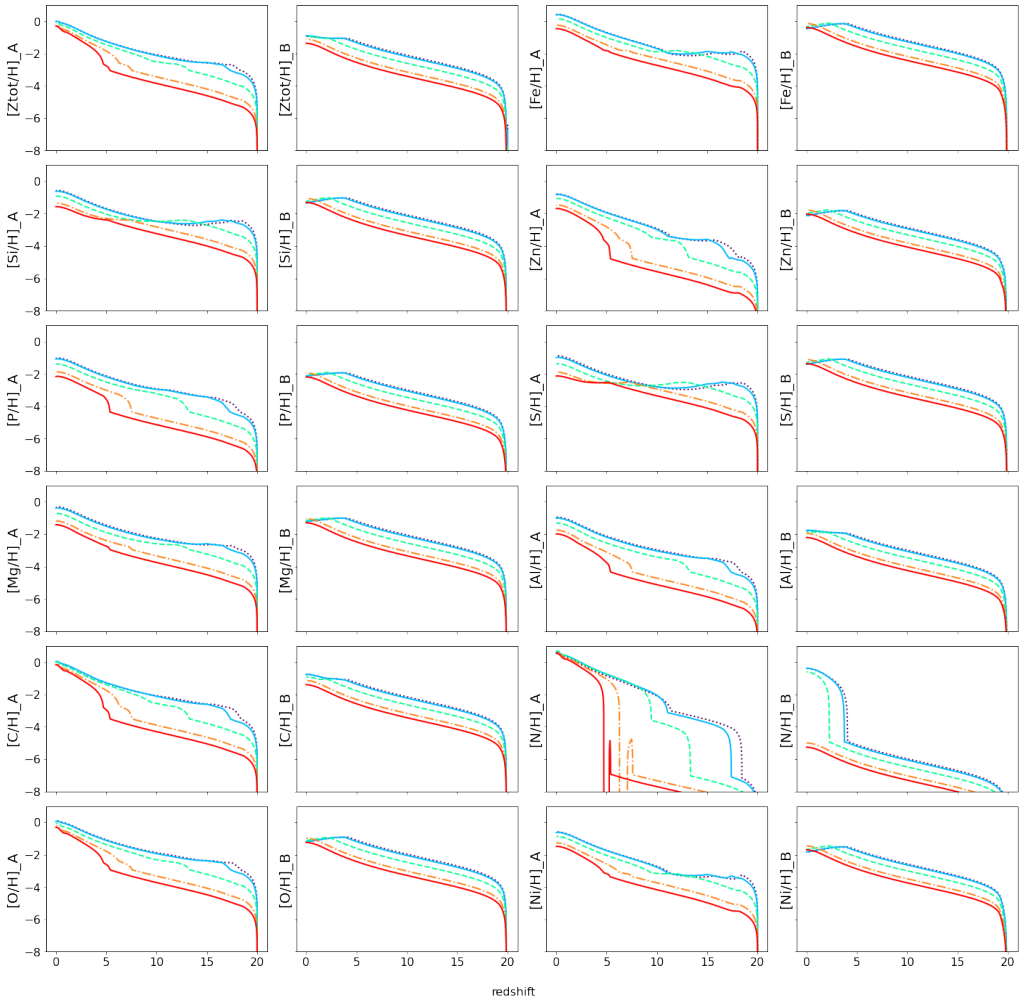

Figure 4.8 - The evolution of [Fe/H] with redshift. Top: Model A (Pop III + Pop II). Bottom: Model B (only Pop II).

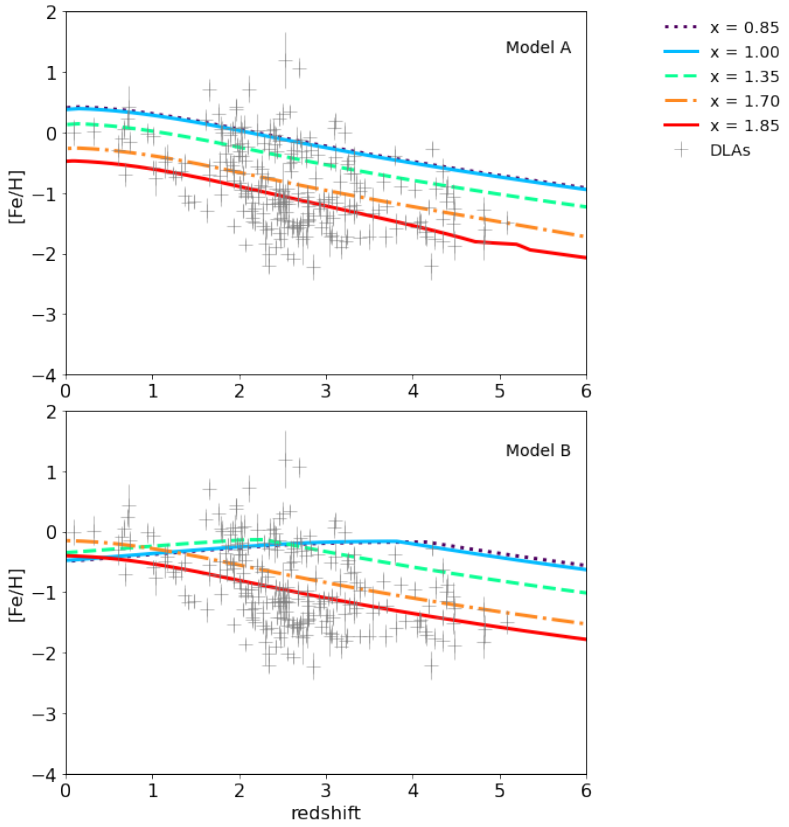

Iron: Fe could be altered by depletion (CIA et al., 2013). Observational abundances could increase by ~ 0.5 dex if depletion is considered in the comparison of the model with DLA data. Details about the methodology used to correct Fe depletion can be checked on Vladilo (2002).

Figure 4.9 - The evolution of [Si/H] with redshift. Top: Model A (Pop III + Pop II). Bottom: Model B (only Pop II).

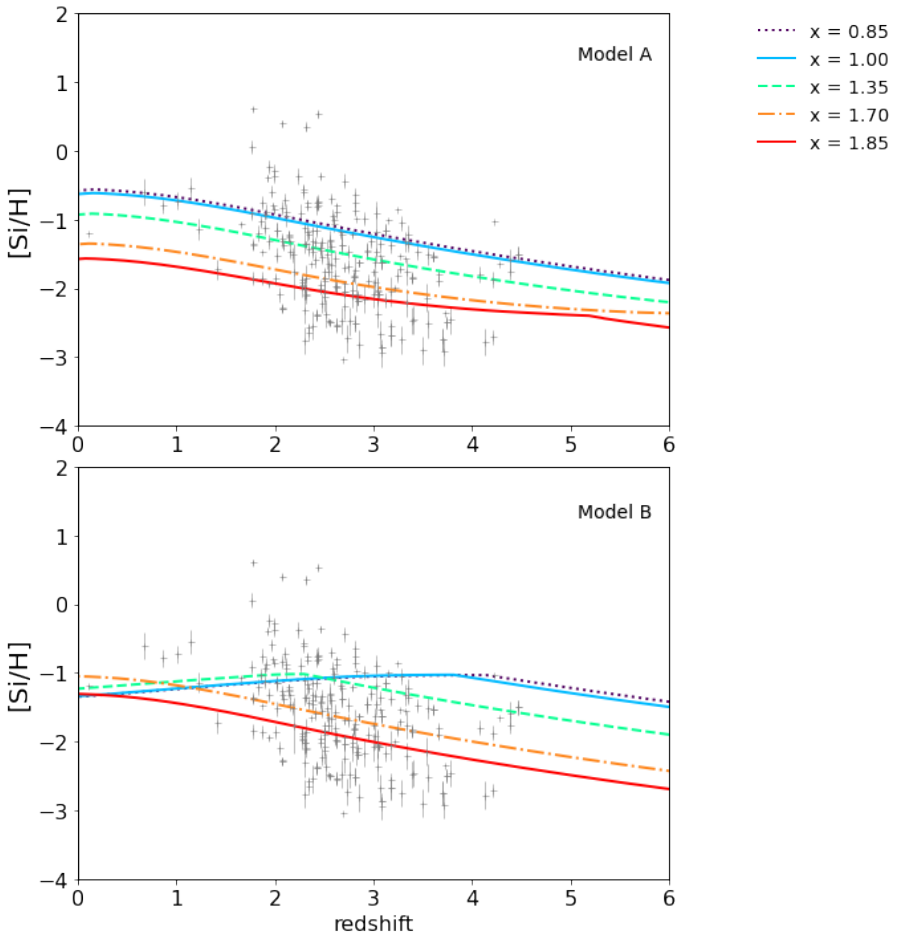

Silicon: Si could be altered by depletion (CIA et al., 2013). Observational abundances could increase by ~ 0.5 dex if depletion is considered in the comparison of the model with DLA data. Details about the methodology used to correct Fe depletion can be checked on Vladilo (2002). Prochaska and Wolfe (2002) shows that although it is a refractory element, its depletion is not strong enough to alter significantly the abundances of DLA systems. Vladilo et al. (2011) shows that Si depletion is mild in the ISM and is expected to be weaker in most DLA systems. The depletion of Fe and Mg are measured for comparisons, and it is found that the mean depletion of Si is almost as high as that of Fe, despite Fe being much more depleted than Si on the galactic ISM. They also explain that Si depletion in DLA systems does not correlate with metallicity, unlike Fe, whose depletion rises along with metallicity increase.

Figure 4.10 - The evolution of [Zn/H] with redshift. Top: Model A (Pop III + Pop II). Bottom: Model B (only Pop II).

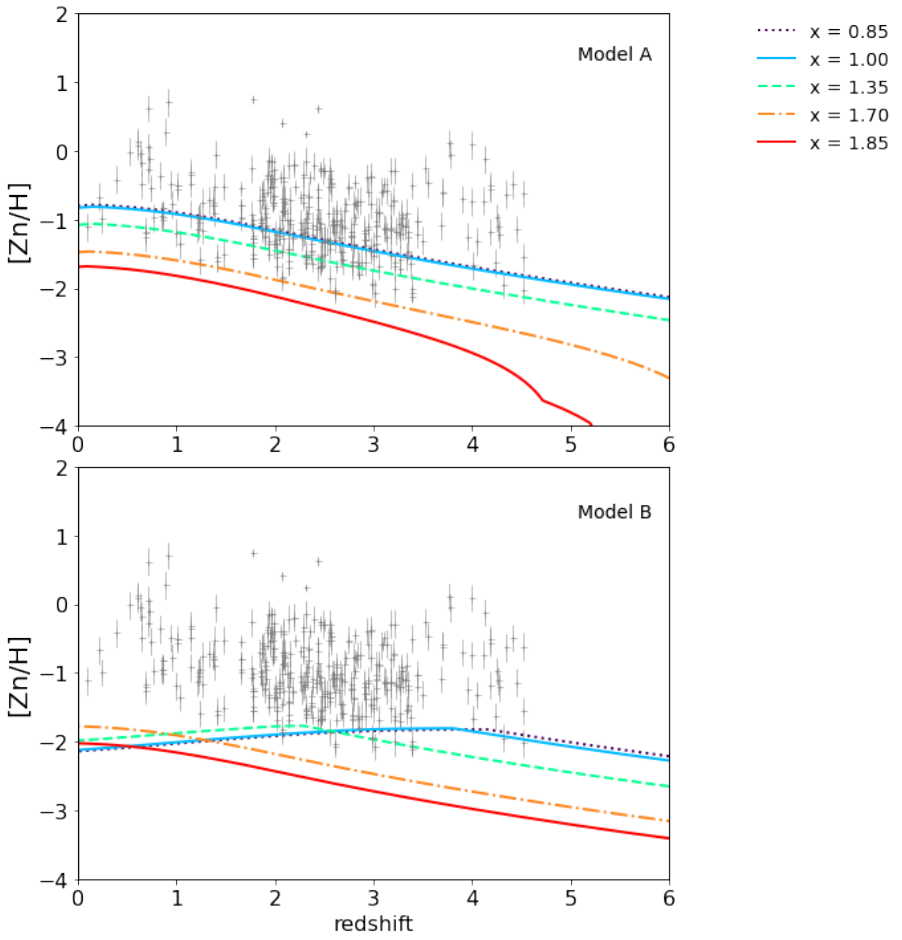

Zinc: Zn is produced mainly in HNe explosions characterized by a more significant production of Zn, Co, V, and Ti than normal SNe (NOMOTO et al., 2006). Stars with $500 - 1000\,M_{\odot}$ produce high amounts of Zn compared to O, C, and other metals (OHKUBO et al., 2006). Kobayashi et al. (2006) suggests that HNe can enhance the production of Zn, and that Zn is considered to be undepleted in DLAs.

Figure 4.11 - The evolution of [Ni/H] with redshift. Top: Model A (Pop III + Pop II). Bottom: Model B (only Pop II).

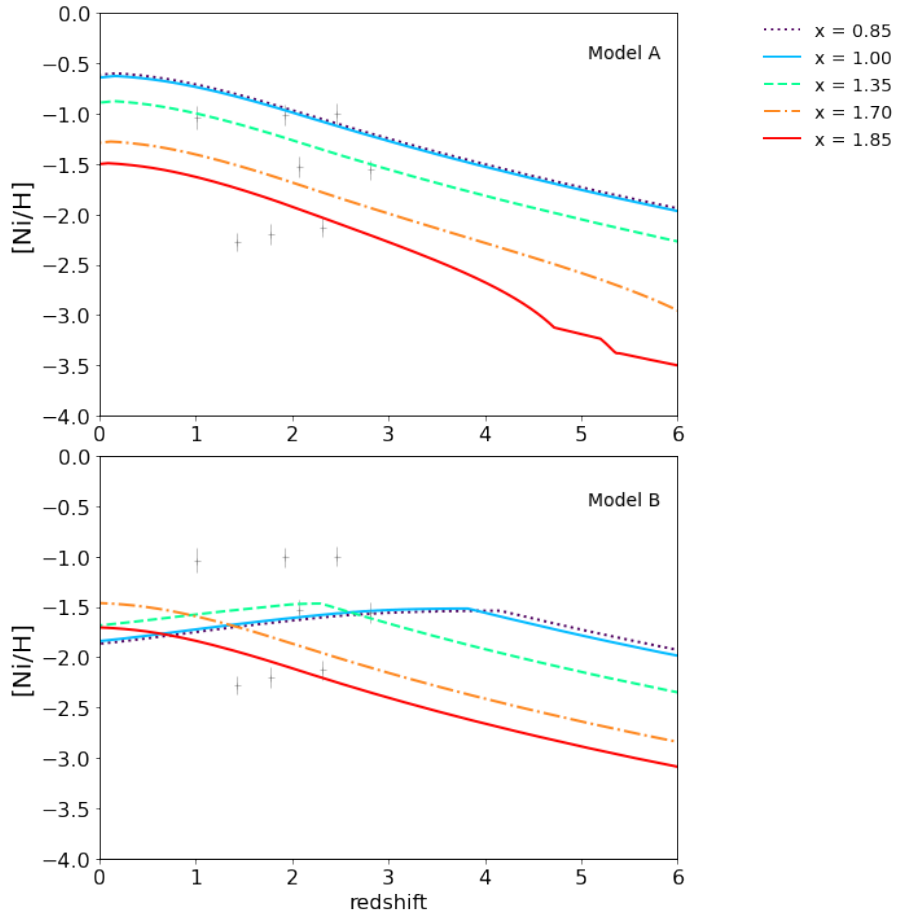

Nickel and Phosphorus: The lack of Ni observations on DLAs poses a challenge in analyzing this element; nevertheless, SNe Ia produces between 4×10^{-3} and $1.4 \times 10^{-2}\,M_{\odot}$ of Ni and from 8.5×10^{-5} to $4 \times 10^{-4}\,M_{\odot}$ of P depending on the specific model (NOMOTO et al., 1997), and it is important to observe the outcome of these types of stars in the present Model.

Figure 4.12 - The evolution of [P/H] with redshift. Top: Model A (Pop III + Pop II). Bottom: Model B (only Pop II).

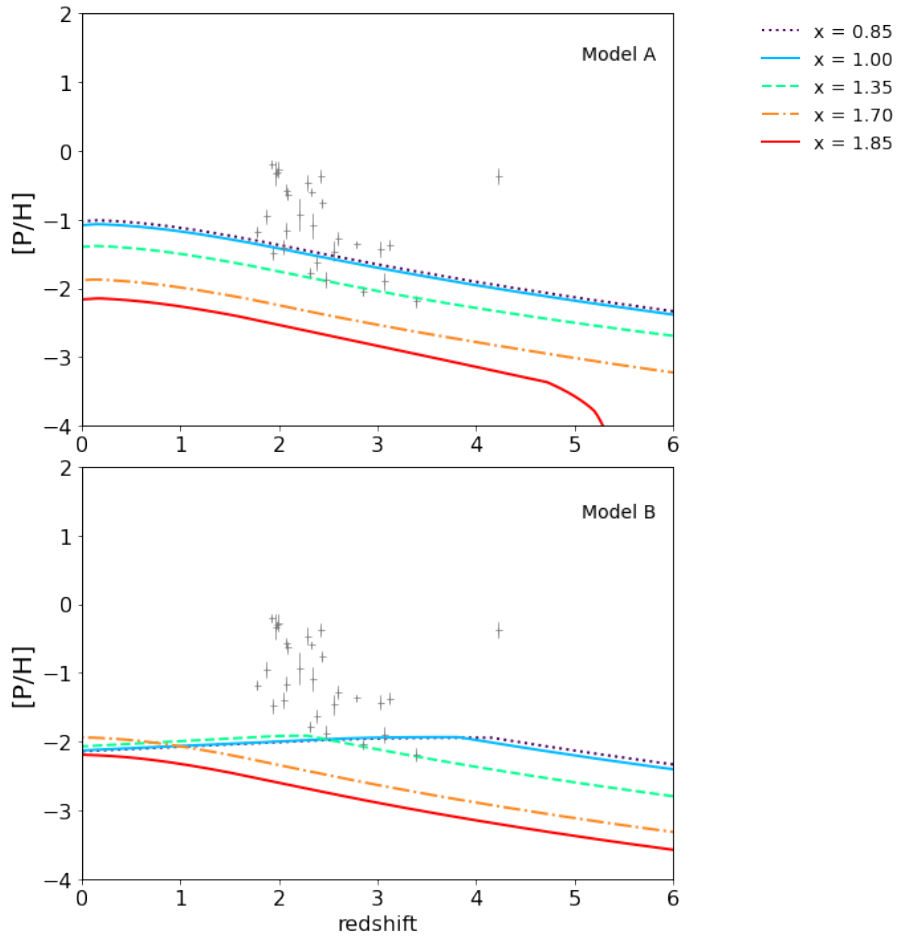

Magnesium: Mg is a refractory element, and its depleting effect must be considered. A challenge that arises in Mg determination comes from the saturation of the doublet used for its characterization, leaving only one possible line to provide Mg abundance. Given the problems related to its determination, current observations should be confirmed by additional Mg measurements to conclude if it could have a particular nucleosynthesis effect in DLA systems (DESSAUGES-ZAVADSKY et al., 2002).

Figure 4.13 - The evolution of [Mg/H] with redshift. Top: Model A (Pop III + Pop II). Bottom: Model B (only Pop II).

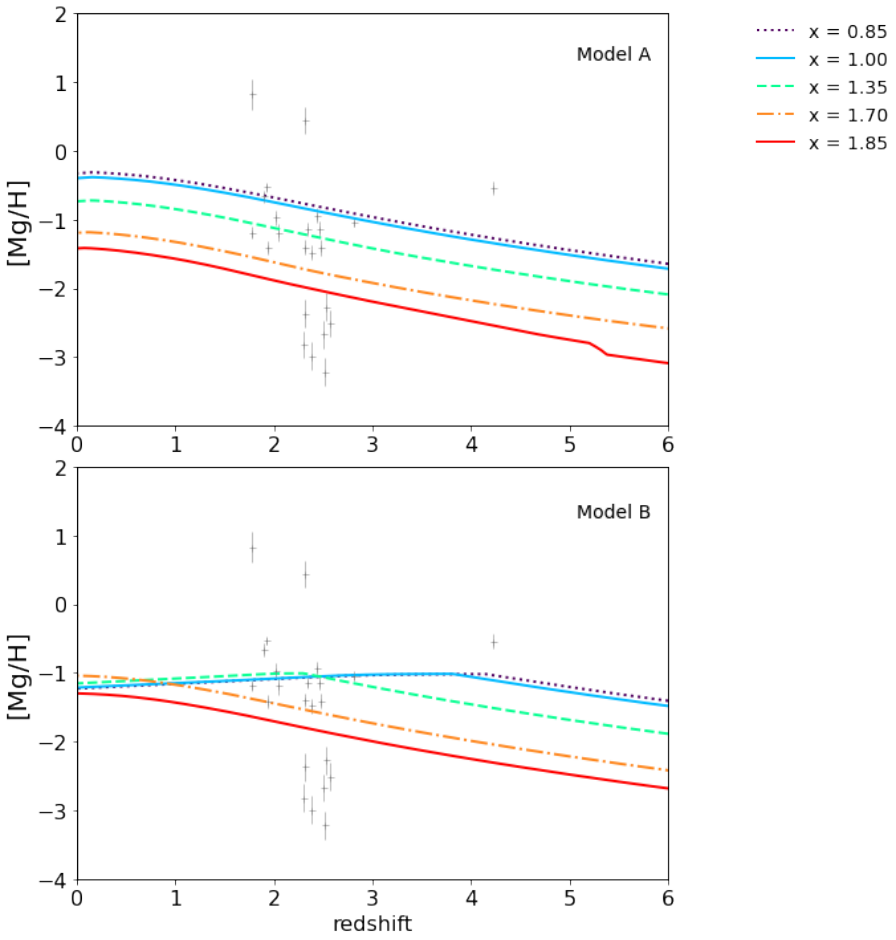

Aluminum: Al has the strongest metal line transition observed in DLAs systems, the Al II λ1670 line (PROCHASKA; WOLFE, 2002), but in the majority of systems, the line is heavily saturated and, together with the blending of lines and blending with the Ly-α forest, determining Al abundances can be a real challenge (DESSAUGES-ZAVADSKY et al., 2003).

Figure 4.14 - The evolution of [Al/H] with redshift. Top: Model A (Pop III + Pop II). Bottom: Model B (only Pop II).

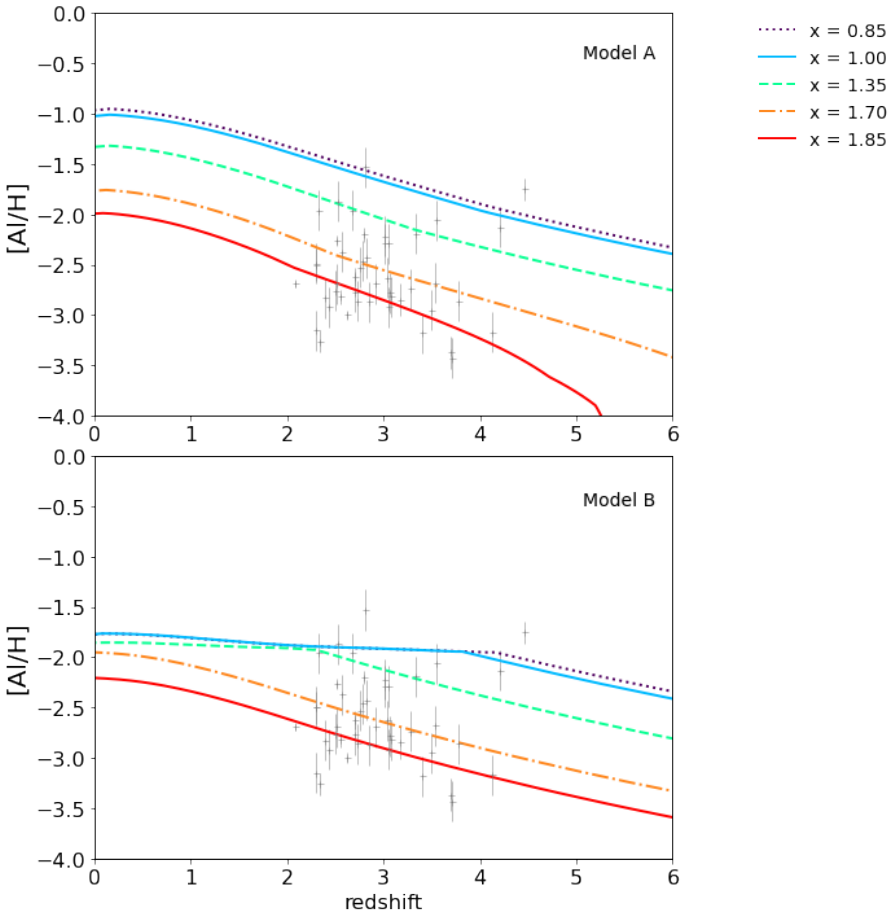

Sulphur: S is considered non-refractory by some authors (PROCHASKA; WOLFE, 2002), but there is still discussion about its actual behavior and if it could be used as a parameter for measuring depletion (JENKINS, 2009; CIA et al., 2016).

Figure 4.15 - The evolution of [S/H] with redshift. Top: Model A (Pop III + Pop II). Bottom: Model B (only Pop II).

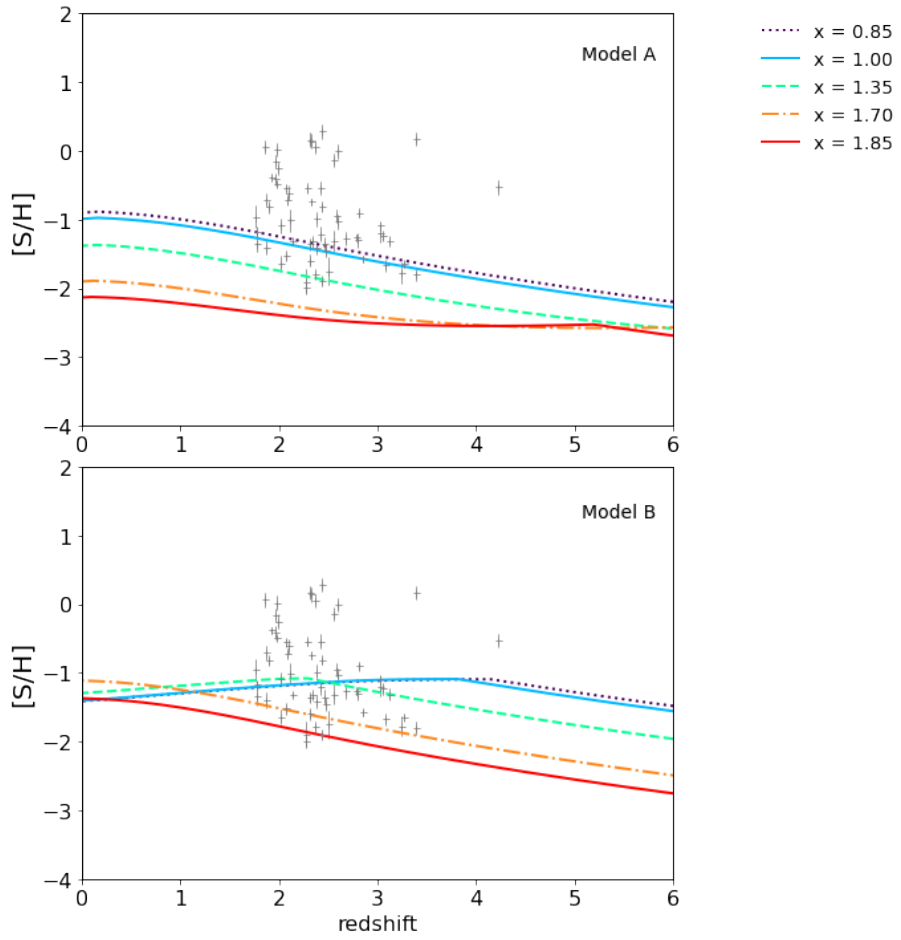

Carbon, Nitrogen, and Oxygen: There is an excess in the abundance of C, N, and O. Regarding depletion effects, O is only mildly refractory according to observations on DLAs and is not highly affected by depletion, although it is challenging to observe once the majority of the lines fall into the Ly-α forest and tend to be saturated (PROCHASKA; WOLFE, 2002). On the other hand, C is considered mildly refractory (PROCHASKA; WOLFE, 2002). Once it is a major constituent of interstellar dust (HENRY et al., 2000; JENKINS, 2009), a substantial part of C could be trapped on dust grains. Also, the lack of observations of C on DLAs is a problem (JENKINS, 2009). N does not exhibit progressively stronger depletions (JENKINS, 2009), and appears to be better represented by model B, i.e., by the behavior of Pop II stars.

Figure 4.16 - The evolution of [C/H], [N/H] and [O/H] with redshift.

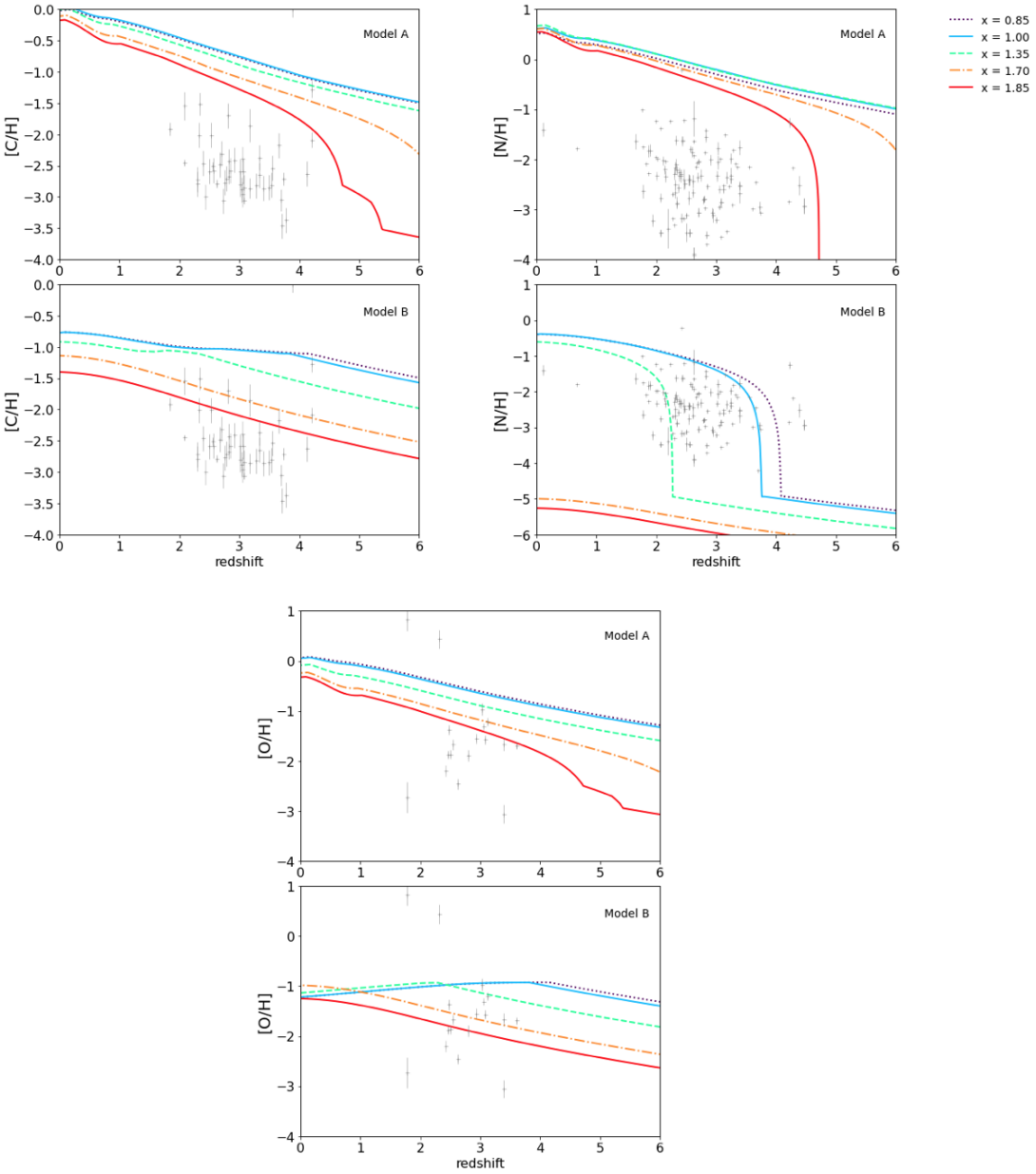

There are, however, other physical processes participating in the C, N, and O production dynamics, which could be interfering with the results. Jenkins (2009) shows that, depending on the case, the consumption of O for producing oxides and silicates is not consistent with results for differential depletion for this element. The lack of O in gas-phase observations is much higher than what is needed for producing these silicates and oxides, and it is very hard to correlate the lack of O on the ISM with models of interstellar grain production. The author suggests that the formation of

compounds involving elements such as H or C could play an important role in taking these elements from the ISM. Therefore, although cooling processes considerably demand C, N, and O for gas cooling and fragmentation, the grain formation processes do not entirely solve the problem for all three overabundant elements. An interesting result from Ioppolo et al. (2008) suggests that O is incorporated in the form of amorphous H_2O ice on the grain surfaces. Work recently developed by Loeb et al. (2016) suggests that there is a possibility that Carbon-Enhanced Metal-Poor stars (CEMPs) from the second generation of stars could host or have hosted planetary systems in their habitable zones. The planets would likely have a major C component in their composition. Also, the degree of C enhancement in CEMP stars has been shown to notably increase as a function of decreasing metallicity (CAROLLO et al., 2012; LOEB, 2018), *i.e.*, the C enhancement in this type of stars is likely much higher in the primordial Universe. Sonnentrucker et al. (2010) also shows that the abundance of water vapor in gas clouds in the Galaxy holds $\sim 0.1\%$ of the available O.

5 CONCLUSIONS AND PERSPECTIVES

The main goal of this work was to investigate the cosmic chemical enrichment through the evolution of chemical elements in the redshift interval $0 \leq z \leq 20$, as well as the contributions of Pop III and Pop II stars to the cosmic enrichment of the Universe. It was achieved by building a cosmic chemical evolution model which couples a semi-analytical cosmological model that computes the CSFR to chemical evolution models for the galactic framework. We computed the evolution of production of Fe, Si, Zn, Ni, P, Mg, Al, S, C, N, O, and compared our results with various observational data sets, the most relevant being DLAs in the redshift interval [0 6] and GCs.

Our main results show that we can consistently model the evolution of cosmic abundances in the Universe using a semi-analytic approach. Also, the 'chemical avalanche' on the primordial Universe, which quickly enriches the medium and provides conditions for Pop II stars to appear, is consistent with the literature on Pop III stars' behavior and chemical evolution models (HEGER; WOOSLEY, 2002; HEGER; WOOSLEY, 2010; TAKAHASHI et al., 2018).

Regarding the behavior of Pop III and Pop II separately, the main difference appears in the behavior of abundances towards $z = 0$. At the same time, **our model considering regular intermediate and high-mass Pop II stars (model B)** shows a decrease in the abundances(except for N and Z_{total}), **while the model including very massive Pop III stars (model A)** reproduces increasing abundances as redshift decreases, which is consistent with observations and similar models in the literature. The latter also offers a better fit of Z_{total} to GC data than the first.

We conclude stating that model A, where the inclusion of Pop III stars appears as the main difference, presents a very good description of mean chemical values across the studied redshift range and the key behavior for the evolution of cosmic abundances in the Universe. Our main results are summarised below:

- The chemical enrichment process in the early Universe occurs very quickly regardless of the stellar population. The pristine Universe reaches $Z = 10^{-6} Z_{\odot}$ in less than 300.000 yr for the mean behavior of Model A (Pop II and Pop III stars), and up to 4.5 Myr for the model with only Pop II stars, depending on the IMF. However, when considering only high mass Pop II stars, the metals are quickly consumed, and the scenario cannot represent chemical abundances at lower redshifts.

- Abundances from GC for Z_{total} are consistently represented by the model with both Pop II and Pop III stars, while the model without Pop III stars is unable to represent observational data, regardless of the IMF.

- Abundances from DLAs for Z_{total} are consistently represented by our model with Pop III and Pop II stars. When comparing the model with abundances corrected for dust depletion and alpha-enhancement, the observations show proper accordance with the model considering both Pop II and Pop III stars, while the model with only Pop II stars cannot account for the behavior of metals towards $z = 0$.

- Regarding the modeling for other elements, there are a few deviations in the results when comparing the models with data from DLAs. However, the combination of mechanisms needed to improve the results is self-completing and can be easily understood, such as the absence of some mechanisms SNe Ia, HNe, dust depletion affecting observational data, and the combination of yields from Pop II stars. HNe and maybe a higher mass branch of stars ($500 - 1000\,M_{\odot}$, Ohkubo et al. (2006)) should improve results for Zn, P, and Ni without raising O and C. In principle, these mechanisms are all consistent with each other and will be studied in a subsequent work.

- The reason for the overabundances of C, N, and O shown in our results remains an open question. New observation focusing on depletion processes in the ISM could explain the overabundances found in the present work (and/or the lack of these elements on the ISM). Considering our results for the other chemical elements, we may suggest the possibility that processes other than (but related to) star formation and evolution could be removing considerable amounts of these elements from the ISM. Once (and if) identified, they will be included in our model.

Altogether, our results indicate that the evolution of chemical abundances in the cosmological framework can be consistently tracked. Our most important result shows that Pop III stars' contribution to the Universe's chemical history should be better understood, and observational campaigns with instruments capable of actually identifying these objects should be seriously considered and implemented. Pop III observations are a long-awaited result, and a firm detection will bring new light to the cosmic history in earlier times.

There are also many ways in which this work can be further developed. Under-

standing the dust depletion of individual elements to correct observational data is necessary to better understand how to advance in the models, once deviations from the simulations are often overlapped with observational challenges. The inclusion of other sources of chemical elements should also be addressed: SNe Ia, HNe, more yields from multiple stars of different masses and metallicities, as well as detailed comparison between the different models for Pop III yields can enrich the results and bring more insights and contributions to the field.

REFERENCES

ABIA, C.; DOMINGUEZ, I.; STRANIERO, O.; LIMONGI, M.; CHIEFFI, A.; ISERN, J. The implications of the new Z = 0 stellar models and yields on the early metal pollution of the intergalactic medium. **The Astrophysical Journal**, v. 557, n. 1, p. 126–136, 2001. ISSN 0004-637X. Available from: <http://stacks.iop.org/0004-637X/557/i=1/a=126>. 30

BLOECKER, T. Stellar evolution of low- and intermediate-mass stars. II. Post-AGB evolution. **Astronomy & Astrophysics**, v. 299, n. 3, p. 755–755, 1995. ISSN 0004-6361. Available from: <http://adsabs.harvard.edu/abs/1995A%26A...299..755B>. 23

BOND, H. E.; NELAN, E. P.; VANDENBERG, D. A.; SCHAEFER, G. H.; HARMER, D. HD 140283: a star in the solar neighborhood that formed shortly after the Big Bang. **The Astrophysical Journal Letters**, v. 765, n. 1, p. L12, mar. 2013. xii, 30, 31, 32

BOUWENS, R. J.; ILLINGWORTH, G. D.; OESCH, P. A.; TRENTI, M.; LABBÉ, I.; FRANX, M.; STIAVELLI, M.; CAROLLO, C. M.; DOKKUM, P. van; MAGEE, D. Lower-luminosity galaxies could reionize the universe: very steep faint-end slopes to the UV luminosity functions at z >= 5-8 from the HUDF09 WFC3/IR observations. **The Astrophysical Journal Letters**, v. 752, n. 1, p. L5, jun. 2012. xi, 15

BOUWENS, R. J.; ILLINGWORTH, G. D.; OESCH, P. A.; FRANX, M.; LABBÉ, I.; TRENTI, M.; DOKKUM, P. van; CAROLLO, C. M.; GONZÁLEZ, V.; SMIT, R.; MAGEE, D. UV-continuum slopes at z ∼4-7 from the HUDF09+ERS+CANDELS observations: discovery of a well-defined UV color-magnitude relationship for z >= 4 star-forming galaxies. **The Astrophysical Journal**, v. 754, n. 2, p. 83, aug. 2012. xi, 15

BROMM, V.; FERRARA, A.; COPPI, P. S.; LARSON, R. B. The fragmentation of pre-enriched primordial objects. **Monthly Notices of the Royal Astronomical Society**, v. 328, n. 3, p. 969–976, dec. 2001. 4

BROMM, V.; LOEB, A. The formation of the first low-mass stars from gas with low carbon and oxygen abundances. **Nature**, v. 425, n. 6960, p. 812–814, oct 2003. ISSN 0028-0836. Available from: <http://www.nature.com/articles/nature02071>. 4

CALURA, F.; MATTEUCCI, F. Cosmic metal production and the mean metallicity of the Universe. **Monthly Notices of the Royal Astronomical Society**, v. 350, n. 1, p. 351–364, may 2004. 9, 34

_____. Cosmic history of star formation and metal production. In: KUBONO, S.; AOKI, W.; KAJINO, T.; MOTOBAYASHI, T.; NOMOTO, K. (Ed.). **Origin of matter and evolution of galaxies**. [S.l.: s.n.], 2006. (American Institute of Physics Conference Series, v. 847), p. 371–373. 9

CALURA, F.; MENCI, N. Chemical evolution of local galaxies in a hierarchical model. **Monthly Notices of the Royal Astronomical Society**, v. 400, n. 3, p. 1347–1365, dec. 2009. 4

CAMPBELL, S. W.; LATTANZIO, J. C. Evolution and nucleosynthesis of extremely metal-poor and metal-free low- and intermediate-mass stars. I. Stellar yield tables and the CEMPs. **Astronomy & Astrophysics**, v. 490, n. 2, p. 769–776, nov. 2008. 2, 22

CAROLLO, D.; BEERS, T. C.; BOVY, J.; SIVARANI, T.; NORRIS, J. E.; FREEMAN, K. C.; AOKI, W.; LEE, Y. S.; KENNEDY, C. R. Carbon-enhanced metal-poor stars in the inner and outer halo components of the milky way. **The Astrophysical Journal**, v. 744, n. 2, p. 195, jan 2012. ISSN 0004-637X. Available from: <https://iopscience.iop.org/article/10.1088/0004-637X/744/2/195>. 47

CARROLL, S. M.; PRESS, W. H.; TURNER, E. L. The cosmological constant. **Annual Review of Astronomy and Astrophysics**, v. 30, p. 499–542, jan. 1992. 8

CASEY, C. M.; BERTA, S.; BÉTHERMIN, M.; BOCK, J.; BRIDGE, C.; BURGARELLA, D.; CHAPIN, E.; CHAPMAN, S. C.; CLEMENTS, D. L.; CONLEY, A.; CONSELICE, C. J.; COORAY, A.; FARRAH, D.; HATZIMINAOGLOU, E.; IVISON, R. J.; FLOC'H, E. le; LUTZ, D.; MAGDIS, G.; MAGNELLI, B.; OLIVER, S. J.; PAGE, M. J.; POZZI, F.; RIGOPOULOU, D.; RIGUCCINI, L.; ROSEBOOM, I. G.; SANDERS, D. B.; SCOTT, D.; SEYMOUR, N.; VALTCHANOV, I.; VIEIRA, J. D.; VIERO, M.; WARDLOW, J. A population of z $>$ 2 far-infrared Herschel-SPIRE-selected starbursts. **The Astrophysical Journal**, v. 761, n. 2, p. 139, dec. 2012. 9

CAYREL, R.; HILL, V.; BEERS, T. C.; BARBUY, B.; SPITE, M.; SPITE, F.; PLEZ, B.; ANDERSEN, J.; BONIFACIO, P.; FRANÇOIS, P.; MOLARO, P.;

NORDSTRÖM, B.; PRIMAS, F. Measurement of stellar age from uranium decay. **Nature**, v. 409, n. 6821, p. 691–692, feb. 2001. xii, 30, 31, 32

CENTURION, M.; BONIFACIO, P.; MOLARO, P.; VLADILO, G. Nitrogen abundances in damped lyα galaxies. **The Astrophysical Journal**, v. 509, n. 2, p. 620–632, dec 1998. ISSN 0004-637X. Available from: <https://iopscience.iop.org/article/10.1086/306537>. 34

CHIEFFI, A.; LIMONGI, M. Explosive yields of massive stars from Z = 0 to Z = Z. **The Astrophysical Journal**, v. 608, n. 1, p. 405–410, jun 2004. ISSN 0004-637X. Available from: <https://iopscience.iop.org/article/10.1086/392523>. 1, 2, 23, 24

CIA, A. D.; LEDOUX, C.; MATTSSON, L.; PETITJEAN, P.; SRIANAND, R.; GAVIGNAUD, I.; JENKINS, E. B. Dust-depletion sequences in damped Lyman- α absorbers. **Astronomy & Astrophysics**, v. 596, p. A97, dec 2016. ISSN 0004-6361. Available from: <http://www.aanda.org/10.1051/0004-6361/201527895>. 34, 44

CIA, A. D.; LEDOUX, C.; PETITJEAN, P.; SAVAGLIO, S. The cosmic evolution of dust-corrected metallicity in the neutral gas. **Astronomy & Astrophysics**, v. 611, p. A76, apr. 2018. xii, 27, 33, 34, 35

CIA, A. D.; LEDOUX, C.; SAVAGLIO, S.; SCHADY, P.; VREESWIJK, P. M. Dust-to-metal ratios in damped Lyman- α absorbers. **Astronomy & Astrophysics**, v. 560, p. A88, dec 2013. ISSN 0004-6361. Available from: <http://www.aanda.org/10.1051/0004-6361/201321834>. 38, 39

COPI, C. J. A stochastic approach to chemical evolution. **The Astrophysical Journal**, v. 487, n. 2, p. 704, 1997. 11

COWAN, J. J.; SNEDEN, C.; BURLES, S.; IVANS, I. I.; BEERS, T. C.; TRURAN, J. W.; LAWLER, J. E.; PRIMAS, F.; FULLER, G. M.; PFEIFFER, B.; KRATZ, K.-L. The chemical composition and age of the metal-poor halo star BD +17°3248. **The Astrophysical Journal**, v. 572, n. 2, p. 861–879, jun. 2002. xii, 30, 31, 32

CUCCIATI, O.; TRESSE, L.; ILBERT, O.; FÈVRE, O. L.; GARILLI, B.; BRUN, V. L.; CASSATA, P.; FRANZETTI, P.; MACCAGNI, D.; SCODEGGIO, M.; ZUCCA, E.; ZAMORANI, G.; BARDELLI, S.; BOLZONELLA, M.; BIELBY, R. M.; MCCRACKEN, H. J.; ZANICHELLI, A.; VERGANI, D. The star

formation rate density and dust attenuation evolution over 12 Gyr with the VVDS surveys. **Astronomy & Astrophysics**, v. 539, p. A31, mar. 2012. xi, 15

DAHLEN, T.; MOBASHER, B.; DICKINSON, M.; FERGUSON, H. C.; GIAVALISCO, M.; KRETCHMER, C.; RAVINDRANATH, S. Evolution of the luminosity function, star formation rate, morphology, and size of star-forming galaxies selected at rest-frame 1500 and 2800 Å. **The Astrophysical Journal**, v. 654, n. 1, p. 172–185, jan. 2007. xi, 15

DAIGNE, F.; OLIVE, K. A.; SILK, J.; STOEHR, F.; VANGIONI, E. Hierarchical growth and cosmic star formation: enrichment, outflows, and supernova rates. **The Astrophysical Journal**, v. 647, n. 2, p. 773–786, aug 2006. Available from: <https://doi.org/10.1086/503092>. 9

DAIGNE, F.; OLIVE, K. A.; VANGIONI-FLAM, E.; SILK, J.; AUDOUZE, J. Cosmic star formation, reionization, and constraints on global chemical evolution. **The Astrophysical Journal**, v. 617, n. 2, p. 693–706, dec. 2004. 25

DAVÉ, R.; OPPENHEIMER, B. D. The enrichment history of baryons in the Universe. **Monthly Notices of the Royal Astronomical Society**, v. 374, n. 2, p. 427–435, 2007. ISSN 00358711. Available from: <http://dx.doi.org/10.1111/j.1365-2966.2006.11177.x>. 4, 33, 34

DESSAUGES-ZAVADSKY, M.; PEROUX, C.; KIM, T.-S.; D'ODORICO, S.; MCMAHON, R. G. A homogeneous sample of sub-damped Lyman alpha systems - I. Construction of the sample and chemical abundance measurements. **Monthly Notices of the Royal Astronomical Society**, v. 345, n. 2, p. 447–479, oct 2003. ISSN 0035-8711. Available from: <https://academic.oup.com/mnras/article-lookup/doi/10.1046/j.1365-8711.2003.06949.x>. 43

DESSAUGES-ZAVADSKY, M.; PROCHASKA, J. X.; D'ODORICO, S. New detections of Mn, Ti and Mg in damped Ly α systems: toward reconciling the dust/nucleosynthesis degeneracy. **Astronomy & Astrophysics**, v. 391, n. 3, p. 801–807, sep 2002. ISSN 0004-6361. Available from: <http://www.aanda.org/10.1051/0004-6361:20020843>. 34, 42

DESSAUGES-ZAVADSKY, M.; ZAMOJSKI, M.; SCHAERER, D.; COMBES, F.; EGAMI, E.; SWINBANK, A. M.; RICHARD, J.; SKLIAS, P.; RAWLE, T. D.; REX, M.; KNEIB, J. P.; BOONE, F.; BLAIN, A. Molecular gas content in strongly lensed z $\sim$1.5-3 star-forming galaxies with low infrared luminosities. **Astronomy & Astrophysics**, v. 577, p. A50, may 2015. xi, 19

DOHERTY, C. L.; GIL-PONS, P.; LAU, H. H. B.; LATTANZIO, J. C.; SIESS, L. Super and massive AGB stars – II. Nucleosynthesis and yields – Z = 0.02, 0.008 and 0.004. **Monthly Notices of the Royal Astronomical Society**, v. 437, n. 1, p. 195–214, nov 2013. ISSN 0035-8711. Available from: <http://academic.oup.com/mnras/article/437/1/195/998013/Super-and-massive-AGB-stars-II-Nucleosynthesis-and>. 2, 23

DOHERTY, C. L.; GIL-PONS, P.; LAU, H. H. B.; LATTANZIO, J. C.; SIESS, L.; CAMPBELL, S. W. Super and massive AGB stars – III. Nucleosynthesis in metal-poor and very metal-poor stars – Z = 0.001 and 0.0001. **Monthly Notices of the Royal Astronomical Society**, v. 441, n. 1, p. 582–598, jun 2014. ISSN 1365-2966. Available from: <http://academic.oup.com/mnras/article/441/1/582/980303/Super-and-massive-AGB-stars-III-Nucleosynthesis-in>. 2, 23

DOTTER, A.; SARAJEDINI, A.; ANDERSON, J. Globular clusters in the outer galactic halo: new Hubble Space Telescope/Advanced Camera for surveys imaging of six globular clusters and the galactic globular cluster age-metallicity relation. **The Astrophysical Journal**, v. 738, n. 1, p. 74, sep. 2011. xii, 30, 32

DVORKIN, I.; SILK, J.; VANGIONI, E.; PETITJEAN, P.; OLIVE, K. A. The origin of dispersion in DLA metallicities. **Monthly Notices of the Royal Astronomical Society**, v. 452, p. L36–L40, sep. 2015. 34

EKSTRÖM, S.; MEYNET, G.; MAEDER, A.; BARBLAN, F. Evolution towards the critical limit and the origin of be stars. **Astronomy & Astrophysics**, v. 478, n. 2, p. 467–485, 2008. Available from: <https://doi.org/10.1051/0004-6361:20078095>. 11

EUROPEAN SPACE AGENCY (ESA). **The history of the Universe**. 2015. Available from: <https://www.esa.int/ESA_Multimedia/Images/2015/02/The_history_of_the_Universe>. Access in: 2022 sep 21. 2

FANG, T.; CEN, R. The transition from population III to population II stars. **The Astrophysical Journal**, v. 616, n. 2, p. L87–L90, dec 2004. ISSN 0004-637X. Available from: <https://iopscience.iop.org/article/10.1086/426786>. 4

FRASER, M.; CASEY, A. R.; GILMORE, G.; HEGER, A.; CHAN, C. The mass distribution of Population III stars. **Monthly Notices of the Royal Astronomical Society**, v. 468, n. 1, p. 418–425, jun. 2017. 9

FREBEL, A.; CHRISTLIEB, N.; NORRIS, J. E.; THOM, C.; BEERS, T. C.; RHEE, J. Discovery of HE 1523-0901, a strongly r-process-enhanced metal-poor

star with detected uranium. **The Astrophysical Journal Letters**, v. 660, n. 2, p. L117–L120, may 2007. xii, 30, 31, 32

FREBEL, A.; NORRIS, J. E. Near-field cosmology with extremely metal-poor stars. **Annual Review of Astronomy and Astrophysics**, v. 53, n. 1, p. 631–688, aug 2015. ISSN 00664146. 30

FROST, C. A.; LATTANZIO, J. C. On the numerical treatment and dependence of the third dredge-up phenomenon. **The Astrophysical Journal**, v. 473, n. 1, p. 383–387, 1996. ISSN 0004-637X. 23

FYNBO, J. P. U.; STARLING, R. L. C.; LEDOUX, C.; WIERSEMA, K.; THÖNE, C. C.; SOLLERMAN, J.; JAKOBSSON, P.; HJORTH, J.; WATSON, D.; VREESWIJK, P. M.; MØLLER, P.; ROL, E.; GOROSABEL, J.; NÄRÄNEN, J.; WIJERS, R. A. M. J.; BJÖRNSSON, G.; CERÓN, J. M. C.; CURRAN, P.; HARTMANN, D. H.; HOLLAND, S. T.; JENSEN, B. L.; LEVAN, A. J.; LIMOUSIN, M.; KOUVELIOTOU, C.; NELEMANS, G.; PEDERSEN, K.; PRIDDEY, R. S.; TANVIR, N. R. Probing cosmic chemical evolution with gamma-ray bursts: GRB 060206 at z = 4.048. **Astronomy & Astrophysics**, v. 451, n. 3, p. L47–L50, jun. 2006. 33, 34

GALLI, D.; PALLA, F. The dawn of chemistry. **Annual Review of Astronomy and Astrophysics**, v. 51, n. 1, p. 163–206, aug 2013. ISSN 0066-4146. Available from: <http://www.annualreviews.org/doi/10.1146/annurev-astro-082812-141029>. 2

GRIBEL, C.; MIRANDA, O. D.; VILAS-BOAS, J. W. Connecting the cosmic star formation rate with the local star formation. **The Astrophysical Journal**, v. 849, n. 2, p. 108, nov 2017. ISSN 1538-4357. Available from: <https://iopscience.iop.org/article/10.3847/1538-4357/aa921a>. 5, 8, 9, 14

GRUPPIONI, C.; POZZI, F.; RODIGHIERO, G.; DELVECCHIO, I.; BERTA, S.; POZZETTI, L.; ZAMORANI, G.; ANDREANI, P.; CIMATTI, A.; ILBERT, O.; FLOC'H, E. L.; LUTZ, D.; MAGNELLI, B.; MARCHETTI, L.; MONACO, P.; NORDON, R.; OLIVER, S.; POPESSO, P.; RIGUCCINI, L.; ROSEBOOM, I.; ROSARIO, D. J.; SARGENT, M.; VACCARI, M.; ALTIERI, B.; AUSSEL, H.; BONGIOVANNI, A.; CEPA, J.; DADDI, E.; DOMÍNGUEZ-SÁNCHEZ, H.; ELBAZ, D.; SCHREIBER, N. F.; GENZEL, R.; IRIBARREM, A.; MAGLIOCCHETTI, M.; MAIOLINO, R.; POGLITSCH, A.; GARCÍA, A. P.;

SANCHEZ-PORTAL, M.; STURM, E.; TACCONI, L.; VALTCHANOV, I.; AMBLARD, A.; ARUMUGAM, V.; BETHERMIN, M.; BOCK, J.; BOSELLI, A.; BUAT, V.; BURGARELLA, D.; CASTRO-RODRÍGUEZ, N.; CAVA, A.; CHANIAL, P.; CLEMENTS, D. L.; CONLEY, A.; COORAY, A.; DOWELL, C. D.; DWEK, E.; EALES, S.; FRANCESCHINI, A.; GLENN, J.; GRIFFIN, M.; HATZIMINAOGLOU, E.; IBAR, E.; ISAAK, K.; IVISON, R. J.; LAGACHE, G.; LEVENSON, L.; LU, N.; MADDEN, S.; MAFFEI, B.; MAINETTI, G.; NGUYEN, H. T.; O'HALLORAN, B.; PAGE, M. J.; PANUZZO, P.; PAPAGEORGIOU, A.; PEARSON, C. P.; PÉREZ-FOURNON, I.; POHLEN, M.; RIGOPOULOU, D.; ROWAN-ROBINSON, M.; SCHULZ, B.; SCOTT, D.; SEYMOUR, N.; SHUPE, D. L.; SMITH, A. J.; STEVENS, J. A.; SYMEONIDIS, M.; TRICHAS, M.; TUGWELL, K. E.; VIGROUX, L.; WANG, L.; WRIGHT, G.; XU, C. K.; ZEMCOV, M.; BARDELLI, S.; CAROLLO, M.; CONTINI, T.; FÉVRE, O. L.; LILLY, S.; MAINIERI, V.; RENZINI, A.; SCODEGGIO, M.; ZUCCA, E. The Herschel PEP/HerMES luminosity function - I. Probing the evolution of PACS selected Galaxies to z 4. **Monthly Notices of the Royal Astronomical Society**, v. 432, n. 1, p. 23–52, jun. 2013. xi, 15

HEGER, A. **Nucleosynthesis (invited review)**. [S.l.]: University of Heidelberg, Aug. 2016. 3

HEGER, A.; WOOSLEY, S. E. The nucleosynthetic signature of population III. **The Astrophysical Journal**, v. 567, n. 1, p. 532–543, mar 2002. ISSN 0004-637X. Available from: <https://iopscience.iop.org/article/10.1086/338487>. 1, 2, 10, 22, 23, 49

_____. Nucleosynthesis and evolution of massive metal-free stars. **The Astrophysical Journal**, v. 724, n. 1, p. 341, 2010. 1, 22, 49

HENRY, R. B. C.; EDMUNDS, M. G.; KOPPEN, J. On the cosmic origins of carbon and nitrogen. **The Astrophysical Journal**, v. 541, n. 2, p. 660–674, oct 2000. ISSN 0004-637X. Available from: <https://iopscience.iop.org/article/10.1086/309471>. 45

HIRANO, S.; YOSHIDA, N. Radiative cooling implementations in simulations of primordial star formation. **Astrophysical Journal**, v. 763, n. 1, p. 52, jan. 2013. 2

HODGE, J. A.; CUNHA, E. da. High-redshift star formation in the Atacama large millimetre/submillimetre array era. **Royal Society Open Science**, v. 7, n. 12, p. 200556, dec. 2020. xi, 17, 18, 19

IGLESIAS, C. A.; ROGERS, F. J. Updated opal opacities. **The Astrophysical Journal**, v. 464, p. 943, jun 1996. ISSN 0004-637X. Available from: <http://adsabs.harvard.edu/doi/10.1086/177381>. 23

IOCCO, F.; MANGANO, G.; MIELE, G.; PISANTI, O.; SERPICO, P. D. Primordial nucleosynthesis: from precision cosmology to fundamental physics. **Physics Reports**, v. 472, n. 1-6, p. 1–76, mar. 2009. 1

IOPPOLO, S.; CUPPEN, H. M.; ROMANZIN, C.; DISHOECK, E. F. van; LINNARTZ, H. Laboratory evidence for efficient water formation in interstellar ices. **The Astrophysical Journal**, v. 686, n. 2, p. 1474–1479, oct. 2008. 47

JENKINS, E. B. A UNIFIED REPRESENTATION OF GAS-PHASE ELEMENT DEPLETIONS IN THE INTERSTELLAR MEDIUM. **The Astrophysical Journal**, v. 700, n. 2, p. 1299–1348, aug 2009. ISSN 0004-637X. Available from: <https://iopscience.iop.org/article/10.1088/0004-637X/700/2/1299>. 44, 45, 46

KARAKAS, A. I. Updated stellar yields from asymptotic giant branch models. **Monthly Notices of the Royal Astronomical Society**, v. 403, n. 3, p. 1413–1425, 2010. ISSN 00358711. 2, 23

KASHIKAWA, N.; NAGAO, T.; TOSHIKAWA, J.; ISHIZAKI, Y.; EGAMI, E.; HAYASHI, M.; LY, C.; MALKAN, M. A.; MATSUDA, Y.; SHIMASAKU, K.; IYE, M.; OTA, K.; SHIBUYA, T.; JIANG, L.; TANIGUCHI, Y.; SHIOYA, Y. A Lyα emitter with an extremely large rest-frame equivalent width of $\sim$900 Å at z = 6.5: a candidate population III-dominated galaxy? **The Astrophysical Journal**, v. 761, n. 2, p. 85, dec. 2012. 1

KISTLER, M. D.; YÜKSEL, H.; BEACOM, J. F.; HOPKINS, A. M.; WYITHE, J. S. B. The star formation rate in the reionization era as indicated by gamma-ray bursts. **The Astrophysical Journal Letters**, v. 705, n. 2, p. L104–L108, nov. 2009. xi, 15

KISTLER, M. D.; YUKSEL, H.; HOPKINS, A. M. The cosmic star formation rate from the faintest galaxies in the unobservable universe. **arXiv e-prints**, p. arXiv:1305.1630, may 2013. xi, 15

KOBAYASHI, C. Galactic and cosmic chemical evolution with hypernovae. In: HILL, V.; FRANCOIS, P.; PRIMAS, F. (Ed.). **From lithium to uranium: elemental tracers of early cosmic evolution**. [S.l.: s.n.], 2005. v. 228, p. 315–321. 2

KOBAYASHI, C.; SPRINGEL, V.; WHITE, S. D. M. Simulations of cosmic chemical enrichment. **Monthly Notices of the Royal Astronomical Society**, v. 376, n. 4, p. 1465–1479, apr 2007. ISSN 0035-8711. Available from: <https://academic.oup.com/mnras/article-lookup/doi/10.1111/j.1365-2966.2007.11555.x>. 4, 33, 34

KOBAYASHI, C.; UMEDA, H.; NOMOTO, K.; TOMINAGA, N.; OHKUBO, T. Galactic chemical evolution: carbon through zinc. **The Astrophysical Journal**, v. 653, n. 2, p. 1145–1171, dec. 2006. 40

KRUMHOLZ, M. R.; MCKEE, C. F. A general theory of turbulence-regulated star formation, from spirals to ultraluminous infrared galaxies. **The Astrophysical Journal**, v. 630, n. 1, p. 250–268, sep. 2005. 14

LARSON, R. B.; TINSLEY, B. M.; CALDWELL, C. N. The evolution of disk galaxies and the origin of S0 galaxies. **The Astrophysical Journal**, v. 237, p. 692–707, may 1980. 4, 5, 21

LILLY, S. J.; CAROLLO, C. M.; PIPINO, A.; RENZINI, A.; PENG, Y. Gas regulation of galaxies: the evolution of the cosmic specific star formation rate, the metallicity-mass-star-formation rate relations, and the stellar content of halos. **The Astrophysical Journal**, v. 772, n. 2, p. 119, jul 2013. ISSN 0004-637X. Available from: <https://iopscience.iop.org/article/10.1088/0004-637X/772/2/119>. 4

LIU, D.; SCHINNERER, E.; GROVES, B.; MAGNELLI, B.; LANG, P.; LESLIE, S.; JIMENEZ-ANDRADE, E.; RIECHERS, D. A.; POPPING, G.; MAGDIS, G. E.; DADDI, E.; SARGENT, M.; GAO, Y.; FUDAMOTO, Y.; OESCH, P. A.; BERTOLDI, F. Automated mining of the ALMA archive in the COSMOS Field (A^3COSMOS). II. Cold molecular gas evolution out to redshift 6. **The Astrophysical Journal**, v. 887, n. 2, p. 235, dec. 2019. 18

LOEB, A. On the habitability of our universe. In: **Consolidation of fine tuning**. [S.l.]: John Templeton Universe, 2018. ArXiv:1606.08926[astro-ph.CO]. 47

LOEB, A.; BATISTA, R. A.; SLOAN, D. Relative likelihood for life as a function of cosmic time. **Journal of Cosmology and Astroparticle Physics**, v. 8, p. 040, aug. 2016. 47

MA, Q.; MAIO, U.; CIARDI, B.; SALVATERRA, R. Constraining the Pop III IMF with high-z GRBs. **Monthly Notices of the Royal Astronomical Society**, v. 466, n. 1, p. 1140–1148, apr. 2017. 9

MA, X.; HOPKINS, P. F.; FAUCHER-GIGUÈRE, C.-A.; ZOLMAN, N.; MURATOV, A. L.; KEREŠ, D.; QUATAERT, E. The origin and evolution of the galaxy mass-metallicity relation. **Monthly Notices of the Royal Astronomical Society**, v. 456, n. 2, p. 2140–2156, feb. 2016. 4

MADAU, P.; DICKINSON, M. Cosmic star-formation history. **Annual Review of Astronomy and Astrophysics**, v. 52, p. 415–486, aug. 2014. 14

MAGNELLI, B.; ELBAZ, D.; CHARY, R. R.; DICKINSON, M.; BORGNE, D. L.; FRAYER, D. T.; WILLMER, C. N. A. Evolution of the dusty infrared luminosity function from z = 0 to z = 2.3 using observations from Spitzer. **Astronomy & Astrophysics**, v. 528, p. A35, apr. 2011. xi, 15

MAGNELLI, B.; POPESSO, P.; BERTA, S.; POZZI, F.; ELBAZ, D.; LUTZ, D.; DICKINSON, M.; ALTIERI, B.; ANDREANI, P.; AUSSEL, H.; BÉTHERMIN, M.; BONGIOVANNI, A.; CEPA, J.; CHARMANDARIS, V.; CHARY, R. R.; CIMATTI, A.; DADDI, E.; SCHREIBER, N. M. F.; GENZEL, R.; GRUPPIONI, C.; HARWIT, M.; HWANG, H. S.; IVISON, R. J.; MAGDIS, G.; MAIOLINO, R.; MURPHY, E.; NORDON, R.; PANNELLA, M.; GARCÍA, A. P.; POGLITSCH, A.; ROSARIO, D.; SANCHEZ-PORTAL, M.; SANTINI, P.; SCOTT, D.; STURM, E.; TACCONI, L. J.; VALTCHANOV, I. The deepest Herschel-PACS far-infrared survey: number counts and infrared luminosity functions from combined PEP/GOODS-H observations. **Astronomy & Astrophysics**, v. 553, p. A132, may 2013. xi, 15

MAIO, U.; CIARDI, B.; DOLAG, K.; TORNATORE, L.; KHOCHFAR, S. The transition from population III to population II-I star formation. **Monthly Notices of the Royal Astronomical Society**, v. 407, n. 2, p. 1003–1015, 2010. ISSN 00358711. 4

MAIO, U.; PÉROUX, C.; CIARDI, B. Atomic and molecular gas from the epoch of reionisation down to redshift 2. **Astronomy & Astrophysics**, v. 657, p. A47, 2022. Available from: <https://doi.org/10.1051/0004-6361/202142264>. xi, 14, 16, 17

MAIO, U.; TESCARI, E. Origin of cosmic chemical abundances. **Monthly Notices of the Royal Astronomical Society**, v. 453, n. 4, p. 3799–3821, nov 2015. ISSN 0035-8711. Available from: <https://academic.oup.com/mnras/article-lookup/doi/10.1093/mnras/stv1714>. 33

MATTEUCCI, F. **The chemical evolution of the Galaxy**. [S.l.]: Springer, 2001. 21

_____. Introduction to galactic chemical evolution. **Journal of Physics: Conference Series**, v. 703, n. 1, p. 012004, apr 2016. ISSN 1742-6588. Available from: <https://iopscience.iop.org/article/10.1088/1742-6596/703/1/012004>. 4, 5

MATTEUCCI, F.; CALURA, F. Early chemical enrichment of the universe and the role of very massive population III stars. **Monthly Notices of the Royal Astronomical Society**, v. 360, n. 2, p. 447–452, 2005. ISSN 00358711. Available from: <http://dx.doi.org/10.1111/j.1365-2966.2005.08908.x>. 4, 30

MEISSNER, U.-G.; METSCH, B. C. Probing nuclear observables via primordial nucleosynthesis. **arXiv e-prints**, p. arXiv:2208.12600, aug. 2022. 1

NAKAMURA, F.; UMEMURA, M. On the initial mass function of population III stars. **The Astrophysical Journal**, v. 548, n. 1, p. 19–32, feb 2001. ISSN 0004-637X. Available from: <https://iopscience.iop.org/article/10.1086/318663>. 9

NOMOTO, K.; IWAMOTO, K.; NAKASATO, N.; THIELEMANN, F.-K.; BRACHWITZ, F.; TSUJIMOTO, T.; KUBO, Y.; KISHIMOTO, N. Nucleosynthesis in type Ia supernovae. **Nuclear Physics A**, v. 621, n. 1-2, p. 467–476, aug 1997. ISSN 03759474. Available from: <https://linkinghub.elsevier.com/retrieve/pii/S0375947497002911>. 41

NOMOTO, K.; TOMINAGA, N.; UMEDA, H.; KOBAYASHI, C.; MAEDA, K. Nucleosynthesis yields of core-collapse supernovae and hypernovae, and galactic chemical evolution. **Nuclear Physics A**, v. 777, p. 424–458, oct 2006. ISSN 03759474. Available from: <https://linkinghub.elsevier.com/retrieve/pii/S0375947406001953>. 40

OHKUBO, T.; UMEDA, H.; MAEDA, K.; NOMOTO, K.; SUZUKI, T.; TSURUTA, S.; REES, M. J. Core-collapse very massive stars: evolution, explosion, and nucleosynthesis of population III 500–1000 M stars. **The Astrophysical Journal**, v. 645, n. 2, p. 1352–1372, jul 2006. ISSN 0004-637X. Available from: <https://iopscience.iop.org/article/10.1086/504578>. 2, 40, 50

OLIVE, K. A.; STEIGMAN, G.; Walker, T. P. Primordial nucleosynthesis: theory and observations. **Physics Reports**, v. 333, p. 389–407, aug. 2000. 1

PEREIRA, E. S.; MIRANDA, O. D. Stochastic background of gravitational waves generated by pre-galactic black holes. **Monthly Notices of the Royal Astronomical Society**, v. 401, n. 3, p. 1924–1932, jan 2010. ISSN 00358711. Available from: <https://academic.oup.com/mnras/article-lookup/doi/10.1111/j.1365-2966.2009.15774.x>. vii, ix, 1, 5, 7, 10, 22

PÉROUX, C.; HOWK, J. C. The cosmic baryon and metal cycles. **Annual Review of Astronomy and Astrophysics**, v. 58, n. 1, p. 363–406, 2020. Available from: <https://doi.org/10.1146/annurev-astro-021820-120014>. xi, 16, 17

PETTINI, M.; ELLISON, S. L.; STEIDEL, C. C.; SHAPLEY, A. E.; BOWEN, D. V. Si and Mn abundances in damped lyα systems with low dust content. **The Astrophysical Journal**, v. 532, n. 1, p. 65–76, mar 2000. ISSN 0004-637X. Available from: <https://iopscience.iop.org/article/10.1086/308562>. 34

PITROU, C.; COC, A.; UZAN, J.-P.; VANGIONI, E. Precision big bang nucleosynthesis with improved helium-4 predictions. **Physics Reports**, v. 754, p. 1–66, sep. 2018. 1

PRESS, W. H.; SCHECHTER, P. Formation of galaxies and clusters of galaxies by self-similar gravitational condensation. **The Astrophysical Journal**, v. 187, p. 425–438, feb. 1974. 7

PROCHASKA, J. X.; WOLFE, A. M. The UCSD HIRES/Keck I damped lyα abundance database. II. The implications. **The Astrophysical Journal**, v. 566, n. 1, p. 68–92, feb 2002. ISSN 0004-637X. Available from: <https://iopscience.iop.org/article/10.1086/338080>. 39, 43, 44, 45

RAFELSKI, M.; WOLFE, A. M.; PROCHASKA, J. X.; NEELEMAN, M.; MENDEZ, A. J. Metallicity evolution of damped lyα systems out to z $\sim$5. **The Astrophysical Journal**, v. 755, n. 2, p. 89, aug. 2012. xii, 33, 35

RAITERI, C. M.; VILLATA, M.; NAVARRO, J. F. Simulations of galactic chemical evolution. I. O and Fe abundances in a simple collapse model. **Astronomy & Astrophysics**, v. 315, p. 105–115, nov. 1996. 11

REDDY, N. A.; STEIDEL, C. C. A steep faint-end slope of the UV luminosity function at z $\sim$2-3: implications for the global stellar mass density and star formation in low-mass halos. **The Astrophysical Journal**, v. 692, n. 1, p. 778–803, feb. 2009. xi, 15

REIMERS, D. Circumstellar absorption lines and mass loss from red giants. **Mémoires de la Société Royale des Sciences de Liège**, v. 8, p. 369–382, 1975. 23

ROBOTHAM, A. S. G.; DRIVER, S. P. The GALEX-SDSS NUV and FUV flux density and local star formation rate. **Monthly Notices of the Royal Astronomical Society**, v. 413, n. 4, p. 2570–2582, jun. 2011. xi, 15

ROLLINDE, E.; VANGIONI, E.; MAURIN, D.; OLIVE, K. A.; DAIGNE, F.; SILK, J.; VINCENT, F. H. Influence of population III stars on cosmic chemical evolution. **Monthly Notices of the Royal Astronomical Society**, v. 398, n. 4, p. 1782–1792, 2009. ISSN 00358711. Available from: <http://dx.doi.org/10.1111/j.1365-2966.2009.15259.x>. 33, 34

SALPETER, E. E. The rate of star formation in the galaxy. **The Astrophysical Journal**, v. 129, n. 1, p. 608, may 1959. ISSN 0004-637X. Available from: <http://adsabs.harvard.edu/doi/10.1086/146660>. 9

SALVADORI, S.; SCHNEIDER, R.; FERRARA, A. Cosmic stellar relics in the galactic halo. **Monthly Notices of the Royal Astronomical Society**, v. 381, n. 2, p. 647–662, oct. 2007. 7

SANTORO, F.; SHULL, J. M. Critical metallicity and fine-structure emission of primordial gas enriched by the first stars. **The Astrophysical Journal**, v. 643, n. 1, p. 26–37, may 2006. ISSN 0004-637X. Available from: <https://iopscience.iop.org/article/10.1086/501518>. 4

SCHAERER, D. On the properties of massive population III stars and metal-free stellar populations. **Astronomy & Astrophysics**, v. 382, n. 1, p. 28–42, jan 2002. ISSN 0004-6361. Available from: <http://www.aanda.org/10.1051/0004-6361:20011619>. 1

SCHIMINOVICH, D.; ILBERT, O.; ARNOUTS, S.; MILLIARD, B.; TRESSE, L.; FÈVRE, O. L.; TREYER, M.; WYDER, T. K.; BUDAVÁRI, T.; ZUCCA, E.; ZAMORANI, G.; MARTIN, D. C.; ADAMI, C.; ARNABOLDI, M.; BARDELLI, S.; BARLOW, T.; BIANCHI, L.; BOLZONELLA, M.; BOTTINI, D.; BYUN, Y. I.; CAPPI, A.; CONTINI, T.; CHARLOT, S.; DONAS, J.; FORSTER, K.; FOUCAUD, S.; FRANZETTI, P.; FRIEDMAN, P. G.; GARILLI, B.; GAVIGNAUD, I.; GUZZO, L.; HECKMAN, T. M.; HOOPES, C.; IOVINO, A.; JELINSKY, P.; BRUN, V. L.; LEE, Y. W.; MACCAGNI, D.; MADORE, B. F.; MALINA, R.; MARANO, B.; MARINONI, C.; MCCRACKEN, H. J.; MAZURE,

A.; MENEUX, B.; MORRISSEY, P.; NEFF, S.; PALTANI, S.; PELLÒ, R.; PICAT, J. P.; POLLO, A.; POZZETTI, L.; RADOVICH, M.; RICH, R. M.; SCARAMELLA, R.; SCODEGGIO, M.; SEIBERT, M.; SIEGMUND, O.; SMALL, T.; SZALAY, A. S.; VETTOLANI, G.; WELSH, B.; XU, C. K.; ZANICHELLI, A. The GALEX-VVDS measurement of the evolution of the far-ultraviolet luminosity density and the cosmic star formation rate. **The Astrophysical Journal Letters**, v. 619, n. 1, p. L47–L50, jan. 2005. xi, 15

SCHINNERER, E.; GROVES, B.; SARGENT, M. T.; KARIM, A.; OESCH, P. A.; MAGNELLI, B.; LEFEVRE, O.; TASCA, L.; CIVANO, F.; CASSATA, P.; SMOLČIĆ, V. Gas fraction and depletion time of massive star-forming galaxies at z ∼3.2: no change in global star formation process out to z > 3. **The Astrophysical Journal**, v. 833, n. 1, p. 112, dec. 2016. xi, 19

_____. _____. **The Astrophysical Journal**, v. 833, n. 1, p. 112, dec. 2016. 14

SCHMIDT, M. The rate of star formation. **The Astrophysical Journal**, v. 129, p. 243, 1959. ISSN 0004-637X. 9

SCHNEIDER, R. The population III/II transition. In: WHALEN, D. J.; BROMM, V.; YOSHIDA, N. (Ed.). **First stars and galaxies: challenges for the next decade**. [S.l.: s.n.], 2010. (AIP Conference Series, v. 1294), p. 102–109. 4

SCHNEIDER, R.; SALVATERRA, R.; FERRARA, A.; CIARDI, B. Constraints on the initial mass function of the first stars. **Monthly Notices of the Royal Astronomical Society**, v. 369, n. 2, p. 825–834, jun. 2006. 9

SCOVILLE, N.; AUSSEL, H.; SHETH, K.; SCOTT, K. S.; SANDERS, D.; IVISON, R.; POPE, A.; CAPAK, P.; BOUT, P. V.; MANOHAR, S.; KARTALTEPE, J.; ROBERTSON, B.; LILLY, S. The evolution of interstellar medium mass probed by dust emission: ALMA observations at z = 0.3-2. **The Astrophysical Journal**, v. 783, n. 2, p. 84, mar. 2014. xi, 19

SCOVILLE, N.; LEE, N.; BOUT, P. V.; DIAZ-SANTOS, T.; SANDERS, D.; DARVISH, B.; BONGIORNO, A.; CASEY, C. M.; MURCHIKOVA, L.; KODA, J.; CAPAK, P.; VLAHAKIS, C.; ILBERT, O.; SHETH, K.; MOROKUMA-MATSUI, K.; IVISON, R. J.; AUSSEL, H.; LAIGLE, C.; MCCRACKEN, H. J.; ARMUS, L.; POPE, A.; TOFT, S.; MASTERS, D. Evolution of interstellar medium, star formation, and accretion at high redshift. **The Astrophysical Journal**, v. 837, n. 2, p. 150, mar. 2017. 18

SCOVILLE, N.; SHETH, K.; AUSSEL, H.; BOUT, P. V.; CAPAK, P.; BONGIORNO, A.; CASEY, C. M.; MURCHIKOVA, L.; KODA, J.; ÁLVAREZ-MÁRQUEZ, J.; LEE, N.; LAIGLE, C.; MCCRACKEN, H. J.; ILBERT, O.; POPE, A.; SANDERS, D.; CHU, J.; TOFT, S.; IVISON, R. J.; MANOHAR, S. ISM masses and the star formation law at Z = 1 to 6: ALMA observations of dust continuum in 145 galaxies in the COSMOS survey field. **The Astrophysical Journal**, v. 820, n. 2, p. 83, apr. 2016. xi, 19

SHETH, R. K.; TORMEN, G. Large-scale bias and the peak background split. **Monthly Notices of the Royal Astronomical Society**, v. 308, n. 1, p. 119–126, sep. 1999. 7

SHU, X. W.; ELBAZ, D.; BOURNE, N.; SCHREIBER, C.; WANG, T.; DUNLOP, J. S.; FONTANA, A.; LEITON, R.; PANNELLA, M.; OKUMURA, K.; MICHAŁOWSKI, M. J.; SANTINI, P.; MERLIN, E.; BUITRAGO, F.; BRUCE, V. A.; AMORIN, R.; CASTELLANO, M.; DERRIERE, S.; COMASTRI, A.; CAPPELLUTI, N.; WANG, J. X.; FERGUSON, H. C. Identification of z $\gtrsim$ 2 Herschel 500 μM sources using color deconfusion. **The Astrophysical Journal Supplement**, v. 222, n. 1, p. 4, jan. 2016. 9

SMITH, M. S.; KAWANO, L. H.; MALANEY, R. A. Experimental, computational, and observational analysis of primordial nucleosynthesis. **The Astrophysical Journal Supplement**, v. 85, p. 219, apr. 1993. 1

SOBRAL, D.; MATTHEE, J.; DARVISH, B.; SCHAERER, D.; MOBASHER, B.; RÖTTGERING, H. J. A.; SANTOS, S.; HEMMATI, S. Evidence for pop III-like stellar populations in the most luminous Ly α emitters at the epoch of reionization: spectroscopic confirmation. **The Astrophysical Journal**, v. 808, n. 2, p. 139, jul 2015. ISSN 1538-4357. Available from: <https://iopscience.iop.org/article/10.1088/0004-637X/808/2/139>. 1

SONNENTRUCKER, P.; NEUFELD, D. A.; PHILLIPS, T. G.; GERIN, M.; LIS, D. C.; LUCA, M. D.; GOICOECHEA, J. R.; BLACK, J. H.; BELL, T. A.; BOULANGER, F.; CERNICHARO, J.; COUTENS, A.; DARTOIS, E.; KAŹMIERCZAK, M.; ENCRENAZ, P.; FALGARONE, E.; GEBALLE, T. R.; GIESEN, T.; GODARD, B.; GOLDSMITH, P. F.; GRY, C.; GUPTA, H.; HENNEBELLE, P.; HERBST, E.; HILY-BLANT, P.; JOBLIN, C.; KOŁOS, R.; KREŁOWSKI, J.; MARTÍN-PINTADO, J.; MENTEN, K. M.; MONJE, R.; MOOKERJEA, B.; PEARSON, J.; PERAULT, M.; PERSSON, C. M.; PLUME, R.; SALEZ, M.; SCHLEMMER, S.; SCHMIDT, M.; STUTZKI, J.; TEYSSIER,

D.; VASTEL, C.; YU, S.; CAUX, E.; GÜSTEN, R.; HATCH, W. A.; KLEIN, T.; MEHDI, I.; MORRIS, P.; WARD, J. S. Detection of hydrogen fluoride absorption in diffuse molecular clouds with Herschel /HIFI: an ubiquitous tracer of molecular gas. **Astronomy & Astrophysics**, v. 521, n. 1, p. L12, oct 2010. ISSN 0004-6361. Available from: <http://www.aanda.org/10.1051/0004-6361/201015082>. 47

SPERA, M.; MAPELLI, M.; BRESSAN, A. The mass spectrum of compact remnants from the PARSEC stellar evolution tracks. **Monthly Notices of the Royal Astronomical Society**, v. 451, n. 4, p. 4086–4103, aug. 2015. 11

SPRINGEL, V.; HERNQUIST, L. The history of star formation in a Λ cold dark matter universe. **Monthly Notices of the Royal Astronomical Society**, v. 339, n. 2, p. 312–334, feb. 2003. 13

STEIGMAN, G. Primordial nucleosynthesis in the precision cosmology era. **Annual Review of Nuclear and Particle Science**, v. 57, n. 1, p. 463–491, nov. 2007. 1

TACCONI, L. J.; GENZEL, R.; SAINTONGE, A.; COMBES, F.; GARCÍA-BURILLO, S.; NERI, R.; BOLATTO, A.; CONTINI, T.; SCHREIBER, N. M. F.; LILLY, S.; LUTZ, D.; WUYTS, S.; ACCURSO, G.; BOISSIER, J.; BOONE, F.; BOUCHÉ, N.; BOURNAUD, F.; BURKERT, A.; CAROLLO, M.; COOPER, M.; COX, P.; FERUGLIO, C.; FREUNDLICH, J.; HERRERA-CAMUS, R.; JUNEAU, S.; LIPPA, M.; NAAB, T.; RENZINI, A.; SALOME, P.; STERNBERG, A.; TADAKI, K.; ÜBLER, H.; WALTER, F.; WEINER, B.; WEISS, A. PHIBSS: unified scaling relations of gas depletion time and molecular gas fractions. **The Astrophysical Journal**, v. 853, n. 2, p. 179, feb. 2018. xi, 18, 19

TAKAHASHI, K.; YOSHIDA, T.; UMEDA, H. Stellar yields of rotating first stars. II. Pair-instability supernovae and comparison with observations. **The Astrophysical Journal**, v. 857, n. 2, p. 111, apr. 2018. 1, 2, 23, 49

TAN, W.-W.; WANG, F. Y.; CHENG, K. S. Constraining warm dark matter mass with cosmic reionization and gravitational waves. **The Astrophysical Journal**, v. 829, n. 1, p. 29, sep 2016. Available from: <https://doi.org/10.3847/0004-637x/829/1/29>. 9

TINSLEY, B. M.; LARSON, R. B. Chemical evolution and the formation of galactic disks. **The Astrophysical Journal**, v. 221, p. 554, apr 1978. ISSN 0004-637X. 4, 5, 21

TORNATORE, L.; FERRARA, A.; SCHNEIDER, R. Population III stars: hidden or disappeared? **Monthly Notices of the Royal Astronomical Society**, v. 382, n. 3, p. 945–950, dec 2007. ISSN 00358711. 4

TORREY, P.; VOGELSBERGER, M.; MARINACCI, F.; PAKMOR, R.; SPRINGEL, V.; NELSON, D.; NAIMAN, J.; PILLEPICH, A.; GENEL, S.; WEINBERGER, R.; HERNQUIST, L. The evolution of the mass-metallicity relation and its scatter in IllustrisTNG. **Monthly Notices of the Royal Astronomical Society**, v. 484, n. 4, p. 5587–5607, apr. 2019. 4

VANGIONI, E.; DVORKIN, I.; OLIVE, K. A.; DUBOIS, Y.; MOLARO, P.; PETITJEAN, P.; SILK, J.; KIMM, T. Cosmological evolution of the nitrogen abundance. **Monthly Notices of the Royal Astronomical Society**, v. 477, n. 1, p. 56–66, jun. 2018. 4, 9, 14, 23, 33, 34

VANZELLA, E.; MENEGHETTI, M.; CAMINHA, G. B.; CASTELLANO, M.; CALURA, F.; ROSATI, P.; GRILLO, C.; DIJKSTRA, M.; GRONKE, M.; SANI, E.; MERCURIO, A.; TOZZI, P.; NONINO, M.; CRISTIANI, S.; MIGNOLI, M.; PENTERICCI, L.; GILLI, R.; TREU, T.; CAPUTI, K.; CUPANI, G.; FONTANA, A.; GRAZIAN, A.; BALESTRA, I. Candidate population III stellar complex at z = 6.629 in the MUSE deep lensed field. **Monthly Notices of the Royal Astronomical Society**, v. 494, n. 1, p. L81–L85, may 2020. 1

VASSILIADIS, E.; WOOD, P. R. Evolution of low- and intermediate-mass stars to the end of the asymptotic giant branch with mass loss. **The Astrophysical Journal**, v. 413, p. 641, aug 1993. ISSN 0004-637X. Available from: <http://adsabs.harvard.edu/doi/10.1086/173033>. 23

VITTI, M. **Uma contribuição ao estudo do enriquecimento químico do universo**. Thesis (Master in Astrophysics). Instituto Nacional de Pesquisas Espaciais. São José dos Campos, SP, Brasil: [s.n.], 2012. 22

VLADILO, G. Chemical abundances of damped ly α systems:. **Astronomy & Astrophysics**, v. 391, n. 2, p. 407–415, aug 2002. ISSN 0004-6361. Available from: <http://www.aanda.org/10.1051/0004-6361:20020822>. 33, 38, 39

VLADILO, G.; ABATE, C.; YIN, J.; CESCUTTI, G.; MATTEUCCI, F. Silicon depletion in damped ly α systems. **Astronomy & Astrophysics**, v. 530, p. A33, jun 2011. ISSN 0004-6361. Available from: <http://www.aanda.org/10.1051/0004-6361/201016330https://ui.adsabs.harvard.edu/abs/2011A&A...530A..33V>. 34, 39

WAGNER-KAISER, R.; MACKEY, D.; SARAJEDINI, A.; CHABOYER, B.; COHEN, R. E.; YANG, S.-C.; CUMMINGS, J. D.; GEISLER, D.; GROCHOLSKI, A. J. Exploring the nature and synchronicity of early cluster formation in the Large Magellanic Cloud - II. Relative ages and distances for six ancient globular clusters. **Monthly Notices of the Royal Astronomical Society**, v. 471, n. 3, p. 3347–3358, nov. 2017. xii, 32

WOLFE, A. M.; GAWISER, E.; PROCHASKA, J. X. Damped lyα systems. **Annual Review of Astronomy & Astrophysics**, v. 43, n. 1, p. 861–918, sep 2005. ISSN 0066-4146. Available from: <http://www.annualreviews.org/doi/10.1146/annurev.astro.42.053102.133950>. 33

WYDER, T. K.; TREYER, M. A.; MILLIARD, B.; SCHIMINOVICH, D.; ARNOUTS, S.; BUDAVÁRI, T.; BARLOW, T. A.; BIANCHI, L.; BYUN, Y.-I.; DONAS, J.; FORSTER, K.; FRIEDMAN, P. G.; HECKMAN, T. M.; JELINSKY, P. N.; LEE, Y.-W.; MADORE, B. F.; MALINA, R. F.; MARTIN, D. C.; MORRISSEY, P.; NEFF, S. G.; RICH, R. M.; SIEGMUND, O. H. W.; SMALL, T.; SZALAY, A. S.; WELSH, B. Y. The ultraviolet galaxy luminosity function in the local universe from GALEX data. **The Astrophysical Journal Letters**, v. 619, n. 1, p. L15–L18, jan. 2005. xi, 15

PUBLICAÇÕES TÉCNICO-CIENTÍFICAS EDITADAS PELO INPE

Teses e Dissertações (TDI)

Teses e Dissertações apresentadas nos Cursos de Pós-Graduação do INPE.

Notas Técnico-Científicas (NTC)

Incluem resultados preliminares de pesquisa, descrição de equipamentos, descrição e ou documentação de programas de computador, descrição de sistemas e experimentos, apresentação de testes, dados, atlas, e documentação de projetos de engenharia.

Propostas e Relatórios de Projetos (PRP)

São propostas de projetos técnico-científicos e relatórios de acompanhamento de projetos, atividades e convênios.

Publicações Seriadas

São os seriados técnico-científicos: boletins, periódicos, anuários e anais de eventos (simpósios e congressos). Constam destas publicações o Internacional Standard Serial Number (ISSN), que é um código único e definitivo para identificação de títulos de seriados.

Pré-publicações (PRE)

Todos os artigos publicados em periódicos, anais e como capítulos de livros.

Manuais Técnicos (MAN)

São publicações de caráter técnico que incluem normas, procedimentos, instruções e orientações.

Relatórios de Pesquisa (RPQ)

Reportam resultados ou progressos de pesquisas tanto de natureza técnica quanto científica, cujo nível seja compatível com o de uma publicação em periódico nacional ou internacional.

Publicações Didáticas (PUD)

Incluem apostilas, notas de aula e manuais didáticos.

Programas de Computador (PDC)

São a seqüência de instruções ou códigos, expressos em uma linguagem de programação compilada ou interpretada, a ser executada por um computador para alcançar um determinado objetivo. Aceitam-se tanto programas fonte quanto os executáveis.